bioRxiv preprint doi: https://doi.org/10.1101/2023.03.03.530942; this version posted March 3, 2023. The copyright holder for this preprint (which was not certified by peer review) is the author/funder, who has granted bioRxiv a license to display the preprint in perpetuity. It is made available under aCC-BY-NC-ND 4.0 International license.

An integrated workflow for quantitative analysis of the newly synthesized proteome

Toman Borteçen[1,2], Torsten Müller[3], and Jeroen Krijgsveld[1,3,*]

[1]German Cancer Research Center (DKFZ), Im Neuenheimer Feld 581, Heidelberg, Germany

[2]Heidelberg University, Faculty of Biosciences, Im Neuenheimer Feld 581, Heidelberg, Germany

[3]Heidelberg University, Medical Faculty, Im Neuenheimer Feld 581, Heidelberg, Germany

*Correspondence to J.K., email j.krijgsveld@dkfz.de, phone: +49-6221-421720

Abstract

The analysis of proteins that are newly synthesized upon a cellular perturbation can provide detailed insight in the proteomic response that is elicited by specific cues. This can be investigated by pulse-labeling of cells with clickable and stable-isotope-coded amino acids for enrichment and mass spectrometric characterization of newly synthesized proteins (NSPs), however convoluted protocols prohibit their routine application. Here we optimized multiple steps in sample preparation, mass spectrometry and data analysis, and integrated them in a semi-automated workflow for the quantitative analysis of the newly synthesized proteome (QuaNPA). Reduced input requirements and data-independent acquisition (DIA) enabled analysis of triple-SILAC-labeled NSP samples, with enhanced throughput while featuring high quantitative accuracy. We applied QuaNPA to investigate the time-resolved cellular response to interferon-gamma (IFNg), observing rapid induction of known and novel targets 2h after IFNg treatment. QuaNPA provides a powerful approach for large-scale investigation of NSPs to gain insight in complex cellular processes.

Introduction

Cells reshape their proteome in response to external stimuli or stress, which occurs throughout the cell's lifetime, e.g. under the influence of growth factors to induce differentiation, or upon genotoxic stress to enhance cell survival or leading to cell death. To investigate these processes, proteome analysis by mass spectrometry, antibodies or aptamers typically is performed to measure differences in overall protein abundance levels between cellular conditions. On the one hand this resolves the concern of transcriptome analysis where accumulating evidence indicates that the correlation between mRNA and protein expression is usually low[1,2]. On the other hand, observing a change in the abundance of a given protein does not indicate the mechanism and dynamics by which this has occurred. Since protein translation is central to rewire protein expression upon cellular perturbations and in disease[3,4], the analysis of protein synthesis is key to fill this gap, in particular because it can reveal immediate changes in the proteome even before this becomes apparent as a change in overall protein abundance[5]. Importantly, measuring these early events, and distinguishing them from proteins exhibiting a secondary or delayed response in protein synthesis, are

bioRxiv preprint doi: https://doi.org/10.1101/2023.03.03.530942; this version posted March 3, 2023. The copyright holder for this preprint (which was not certified by peer review) is the author/funder, who has granted bioRxiv a license to display the preprint in perpetuity. It is made available under aCC-BY-NC-ND 4.0 International license.

crucial to gain insight in the underlying mechanisms that translate a cellular perturbation into a proteomic response.

Experimentally, protein synthesis has been investigated by ribosome profiling, inferring protein translation by genome-wide sequencing of ribosome occupancy sites in mRNA (Ribo-seq). This can be combined with global RNA sequencing to obtain a measure for translation efficiency (TE) by accounting for changes in mRNA expression[6]. Yet, Ribo-seq determines protein translation only indirectly by sequencing of RNA, and it comes with a number of caveats especially when studying cellular perturbation by requiring rigorous statistical methods to faithfully calculate differences in TE[7,8], and by the need to disregard inactive ribosomes that do not contribute to translation[9].

Therefore, a number of mass spectrometry-based proteomic methods have been developed to identify newly synthesized proteins (NSPs) directly at the protein level[10,11], based on incorporation of puromycin (or its derivatives), isotope-labelled amino acids, non-natural amino acids, or combinations thereof[12,13]. Puromycin is incorporated into nascent chains, leading to termination of protein translation and release of the truncated polypeptide which can next be isolated via biotin-streptavidin[14] enrichment, click-chemistry[15] [16,17] or anti-puromycin antibodies[18], depending on the type of puromycin-analogue that is used. This can be combined with stable isotope labelling with amino acid in cell culture (SILAC) to distinguish NSPs from pre-existing or contaminating proteins by subsequent mass spectrometric analyses. Pulsed-SILAC (pSILAC) labelling alone can also be used to label and analyse full-length NSPs that have undergone natural translation termination. As a third approach, non-natural methionine analogues such as L-azidohomoalanine (AHA)[19], L-homopropargylglycine (HPG)[20] or L-azidonorleucine (ANL)[21] can be incorporated into nascent proteins by the cell's translational machinery, exploiting their bio-orthogonal alkyne or azide moieties for subsequent coupling of NSPs to immobilized tags[22], to biotin-conjugates[23], phosphonate alkynes[24] or directly to clickable beads[25]. This covalent (or near-covalent in case of streptavidin) capture of NSPs has the great advantage to allow stringent washing to remove pre-existing (i.e. non-labelled) proteins and other contaminants before digestion of NSPs off the beads and analysis by liquid chromatography coupled to mass spectrometry (LC-MS).

Several strategies have combined the use of clickable and isotope-labelled amino acids to enrich and quantify NSPs in the same experiment. This includes the use of isotope-labelled AHA for the quantification newly synthesized AHA-containing peptides[26], or the simultaneous pulse-labelling of cells with AHA and SILAC amino acids[12,13,27,23]. An important advantage of these strategies is that the detection of isotope-labelled peptides are used as formal evidence for their assignment as NSPs, and to allow relative quantification of NSPs between conditions. These approaches have been applied to investigate proteome response in various model systems including cell culture[28,29,30], in T cells[23], and in mouse tissue both ex vivo[31] and in vivo[32]. In our own work we have combined AHA and pSILAC labelling in various biological contexts e.g. to investigate secreted proteins[27,33], to determine proteomic effects of rRNA methylation[34,35], and to identify effectors of transcriptional regulators[36], thus illustrating broad applicability. In addition, time-

bioRxiv preprint doi: https://doi.org/10.1101/2023.03.03.530942; this version posted March 3, 2023. The copyright holder for this preprint (which was not certified by peer review) is the author/funder, who has granted bioRxiv a license to display the preprint in perpetuity. It is made available under aCC-BY-NC-ND 4.0 International license.

course analysis of macrophage activation showed that robust changes in NSPs can be detected on shorter time scales than in conventional proteome profiling or by the use of pSILAC without NSP enrichment[5].

Despite conceptual advantages, bio-orthogonal NSP enrichment approaches are limited in one or multiple ways with regard to throughput, required input amounts, manual and multi-step sample preparation, and proteomic depth[26,28,29]. For instance, relatively large sample input is needed to isolate the usually small fraction of NSPs, and peptide fractionation or long LC gradients are needed prior to LC-MS to achieve sufficient proteome coverage, however leading to reduced throughput [5,14,17]. To avoid manual sample processing via extensive enrichment protocols, two automated enrichment methods have been developed recently, although they still include lengthy off-deck de-phosphorylation and dialysis steps, while requiring large sample input and reporting limited proteome coverage[24,37]. Additional multiplexing with isobaric tags has been used to increase throughput, but still requires offline sample fractionation and prolonged LC-MS measurement time to achieve sufficient proteomic depth[30,38,39].

Recently, mass spectrometry via data-independent acquisition (DIA) has become a powerful alternative for conventional data-dependent acquisition (DDA) methods for deep proteome profiling in single-shot analyses[40]. Although DIA is directly compatible with label-free quantification, it has been scarcely applied in combination with SILAC labelling because of challenges in data analysis[41,42,43]. Recently, plexDIA was introduced in the DIA-NN environment, demonstrating deep proteome coverage and quantitative accuracy for the analysis of multiplexed samples with non-isobaric labels (mTRAQ)[44]. Conceptually, plexDIA could also be applied to SILAC-labelled samples, in particular for the analysis of NSPs.

Here we addressed these various challenges in the analysis of NSPs, improving multiple steps in sample preparation, mass spectrometry and data analysis that we integrated in an efficient workflow named QuaNPA (Quantitative Newly synthesized Proteome Analysis). QuaNPA is centred around automated enrichment, clean-up and digestion of clickable NSPs on a liquid handling robot, which we facilitated by designing novel high-capacity magnetic alkyne agarose (MAA) beads. Through the use of MAA beads, required protein input was significantly reduced, allowing cells to be grown in 6-well plates, thus making large-scale cell culture experiments a manageable task. Finally, we established that plexDIA enabled the analysis of triple-SILAC-labelled NSP samples by DIA, with quantitative accuracy equivalent to DDA. Importantly, this can be performed in single LC-MS runs, obviating the need for offline peptide fractionation, and thereby achieving a significant increase in throughput. We demonstrate the utility of QuaNPA in a time-series experiment to investigate cellular response to interferon-gamma (IFNg), showing expression of known and novel IFNg response proteins among NSPs at distinct time points, and as early as 2h after addition of IFNg. Collectively, QuaNPA presents a unified approach for systematic NSP analyses across multiple cellular conditions, to understand perturbation-induced proteome responses.

bioRxiv preprint doi: https://doi.org/10.1101/2023.03.03.530942; this version posted March 3, 2023. The copyright holder for this preprint (which was not certified by peer review) is the author/funder, who has granted bioRxiv a license to display the preprint in perpetuity. It is made available under aCC-BY-NC-ND 4.0 International license.

Results

Developing an improved workflow for proteome-wide analysis of newly synthesized proteins

We developed a complete workflow for quantitative newly synthesized proteome analysis (coined QuaNPA), that integrates metabolic labelling of cells, cell lysis, enrichment of newly synthesized proteins, sample clean-up, LC-MS measurement, and data analysis. Here, we have optimized multiple aspects of these individual steps and adapted them for automated processing, with a focus on reducing sample input, and on increasing proteomic depth and sample throughput (Figure 1).

Optimizing the automated enrichment of newly synthesized proteins with magnetic alkyne agarose beads

At the core of the QuaNPA workflow is the metabolic labelling of cells, to incorporate AHA and SILAC amino acids for the capture and quantification, respectively, of newly synthesized proteins (NSPs). To enable efficient and automated enrichment of AHA-containing NSPs, magnetic beads with high density of terminal alkyne groups are beneficial. Since commercially available magnetic alkyne beads lack capacity (30-50 nmol/mg beads), while regular alkyne agarose beads have a high capacity (10-20 µmol/mL resin) but lack magnetic properties to permit automation, we combined the benefit of both by producing magnetic alkyne agarose (MAA) beads by coupling epoxy-activated magnetic agarose with propargylamine. This can be performed in a one-step reaction to generate a large batch for multiple enrichment experiments (Figure 2). Next, we established a protocol on a Bravo liquid handling system to perform enrichment of newly synthesized proteins via click-chemistry in a semi-automated fashion, using MAA-beads and a magnetic rack. The automated protocol is carried out using a 96-well PCR plate, enabling the parallel processing of 8-96 samples including dispensing of reagents, click-based coupling of NSPs to MAA-beads, and stringent washing steps, all in a volume of <200 µL per sample. Next, enriched NSPs are digested off the beads by trypsin, followed by peptide purification using the autoSP3 protocol[45]. To enable the dilution of the tryptic peptides to >95 % acetonitrile, samples were lyophilized after digestion prior to the addition of magnetic SP3-beads and acetonitrile. The automated SP3 peptide clean-up protocol was run on the same Bravo liquid handling platform after exchange of the “reagent” plate to a new 96-well plate (“recovery plate”) for the transfer of purified peptides (Supplementary figure 1) for subsequent proteomic analysis.

To determine the best conditions for the use of MAA beads in the automated enrichment protocol, we generated a pulse-labelled sample and performed enrichment experiments with different amounts of MAA beads and protein input. Specifically, Hela cells were labelled with AHA and intermediate- or heavy SILAC amino acids for 4 h, and 100 µg of protein lysate was used as input for NSP enrichment with different amounts of MAA beads (2-8 µl bead volume per reaction, corresponding to 1.1-4.3 % (v/v)). Although we did not compare different biological conditions at this point, we used both heavy and intermediate SILAC labels to accurately simulate the composition of such newly synthesized proteome samples. As a metric to

bioRxiv preprint doi: https://doi.org/10.1101/2023.03.03.530942; this version posted March 3, 2023. The copyright holder for this preprint (which was not certified by peer review) is the author/funder, who has granted bioRxiv a license to display the preprint in perpetuity. It is made available under aCC-BY-NC-ND 4.0 International license.

assess the efficiency of the newly synthesized proteome enrichment, we compared the ratio of the heavy or intermediate SILAC-labelled precursor peptide ions (i.e. that originate from NSPs), over the unlabelled precursors (i.e. that originate from pre-existing proteins). We observed that slightly more proteins were quantified in enriched compared to non-enriched samples (Figure 3A, Supplementary Data 1). More importantly, the ratio of newly synthesized over pre-existing proteins was 0.25 without enrichment (i.e. -2 on log scale), while this was on average 6.5 (2.7 on log2 scale) after capture of NSPs across all tested amounts of MAA beads (Figure 3B), thus indicating a >25-fold enrichment of NSPs. In addition, this resulted in improved accuracy of NSP quantification in the enriched samples, determined by comparing the distribution of SILAC ratios around the expected ratio (Figure 3C). The quantitative precision, determined by the coefficient of variation (CV) values of the SILAC ratios, was also significantly improved in enriched NSP samples (Figure 3D).

Although the efficiency of the click chemistry-based enrichment with the presented protocol is high, we note that the use of SILAC labels is essential to distinguish genuine NSPs from non-labelled proteins that cannot be fully removed, despite stringent washing (Figure 3A and Supplementary figure 2 A). 'Stickyness' of unlabelled proteins does not depend on protein abundance or hydrophobicity, since both parameters span the same full range as observed for NSPs (Supplementary figure 2A and B), and therefore this cannot be used to exclude them from the analysis.

In addition to the comparison of different MAA bead amounts, the same sample was used to test the influence of protein input amount at a constant MAA bead volume of 4 µL (2.1% (v/v)). Across the range of tested protein input amounts (1-300 µg), we observed a consistently high ratio of SILAC labelled over unlabelled precursor intensities, indicating that the automated enrichment is efficient, even with low protein input (Figure 3E, Supplementary Data 2). As expected, the number of identified proteins scaled with input amount, achieving >3200 proteins at 50 µg of total protein input and reaching a plateau at approximately 3600 proteins from 100 µg and upwards (Figure 3F). These results indicate that 50-100 µg protein input suffices to maximize the number of identifications (at least for the chosen LC gradient length and MS method), and that this can be scaled down to 10 µg or less for scarce samples without a major reduction in efficiency of NSP enrichment.

Collectively, these data indicate that MAA beads permit efficient enrichment of NSPs in an automated fashion over a wide range of protein input amounts, allowing the quantification of a larger number of NSPs with greater precision and accuracy compared to non-enriched samples. In addition, consistent performance across a range of bead quantities indicates that the approach tolerates potential variation in the amount of beads, thus contributing to experimental robustness.

bioRxiv preprint doi: https://doi.org/10.1101/2023.03.03.530942; this version posted March 3, 2023. The copyright holder for this preprint (which was not certified by peer review) is the author/funder, who has granted bioRxiv a license to display the preprint in perpetuity. It is made available under aCC-BY-NC-ND 4.0 International license.

Using plexDIA for newly synthesized proteome analysis

In addition to the described improvements of the newly synthesized proteome sample preparation via the automated enrichment with MAA beads, we tested whether the use of data-independent acquisition (DIA) is advantageous over the use of the data-dependent analysis (DDA) used above. Increasing evidence indicates that DIA achieves increased proteome coverage in label-free approaches, however lack of suitable data analysis tools has prevented its use in combination with non-isobaric labelling methods. This has changed with the newly-developed plexDIA[44] feature of the DIA-NN software[46] that was shown to maintain quantitative accuracy for mTRAQ-labelled samples compared to label-free analysis[44]. We therefore aimed to test the performance of DIA-based MS and plexDIA for the analysis of SILAC-labelled samples, and in particular for NSPs. To this end, we prepared two benchmark samples with defined ratios of SILAC-labelled Hela cell lysates for comparative analysis via a conventional DDA method and two DIA methods. The first sample (mix1) consisted primarily of light protein (70%), with only a smaller fraction of intermediate- and heavy labelled proteins, mimicking a conventional pulse-labelled sample without enrichment. The second sample (mix2) consisted of a smaller fraction of light proteins (20%), with a major contribution of labelled protein, thus mimicking an enriched newly synthesized proteome sample (Figure 4A). Since, in contrast to DDA, both MS1- and MS2-based quantitative data can be used for the analysis of the DIA measurements, two DIA methods were designed: DIA method 1 (DIA m1) was optimized for short cycle time and MS2-based quantification, whereas DIA method 2 (DIA m2) was optimized for MS1-based quantification by including additional high-resolution MS1 scans, resulting in a slightly increased cycle time (Figure 4B, see methods for details). The same LC method was used in all cases. To conduct a thorough comparison of the different acquisition methods, samples, and analysis software, we determined the number of protein identifications, quantitative precision and accuracy for each of the analyses.

The DDA approach consistently quantified fewer proteins than either of the DIA methods in both samples (Figure 4C, Supplementary Data 3). In addition, this number was constant among all L/M/H ratios, indicating that the ability to quantify is independent of the abundance of each of these channels (within the tested range). A number of observations can be made in the DIA data: first, more proteins were quantified in mix2 than in mix1, possibly explained by the difficulty that plexDIA has to quantify the more extreme ratios in mix 1. Second, the number of quantified proteins varied depending on the SILAC channels. Notably, fewer proteins were quantified in cases where the lower abundance channel was involved (H and M in mix 1, L in mix2). These observations suggest that those proteins are credited that occur in higher abundance, and at a ratio closer to 1. This is as expected, since it is more difficult to quantify signals at low S/N ratio, and the gained proteins in the DIA data compared to DDA are likely to be in the lower abundance range in the first place. Third, quantification by MS1 (blue) and MS2 (red) produced very similar numbers of quantified proteins, with a slight tendency for more identifications by MS2 quantification, which was observed both in DIA m1 and m2. Finally, one of the most striking observations from the data is that the number of H/M-quantified proteins in mix2 more than doubled from approximately 3000 in DDA to well over 6000 in DIA

bioRxiv preprint doi: https://doi.org/10.1101/2023.03.03.530942; this version posted March 3, 2023. The copyright holder for this preprint (which was not certified by peer review) is the author/funder, who has granted bioRxiv a license to display the preprint in perpetuity. It is made available under aCC-BY-NC-ND 4.0 International license.

(Figure 4C), indicating a favourable scenario for newly synthesized proteome samples that are dominated by these two SILAC labels (also see Figure 3A).

In addition to the number of quantified proteins, the precision of the quantified protein groups was compared using CV values (Figure 4D). All median CVs were in a narrow range between 5-15%, indicating excellent precision across all data acquisition methods. Yet some subtle trends were observed, where quantification by DDA was more precise in mix2 than in mix1, possibly because ratios were less extreme. Quantitative precision in the two DIA methods at the MS1 level (blue) was highly comparable both for mix1 and mix2 (11-15%), with a tendency for improved precision by DIA m2, likely benefiting from the additional MS1 scans that were included in the method for this purpose. Clearly MS2-based quantification (red) yields data with even greater precision, and the lowest CV (5.4%) was obtained for H/M ratio with the MS2-optimized DIA method (Figure 4D). Next, to assess the accuracy of protein quantification, SILAC ratios were plotted and compared to the expected ratios of the benchmark samples (Figure 4E). The accuracy of the MS1-based quantification data (blue) from both DIA methods is comparable to the DDA data, but also includes larger numbers of outlier values. As observed for precision above, the accuracy is greater for less extreme SILAC ratios, and best accuracy was achieved for MS2-based quantification of 1:1 ratios (H/M) both in mix1 and mix2, which actually produced the most accurate data across the entire data set (Figure 4E).

Overall, this benchmark dataset indicates that DIA measurements of SILAC labelled samples, in combination with the plexDIA functionalities of DIA-NN, yields high quality data with drastically increased proteomic depth and robust quantification. This approach benefits from the large fraction of labelled peptides in the samples, making it highly suitable for the analysis of enriched NSP samples.

Using QuaNPA for the analysis of newly synthesized proteome changes in response to IFNg

Having established QuaNPA as an optimized workflow for newly synthesized proteome analysis that includes the generation of magnetic alkyne beads, conditions for automated protein capture and clean-up, DIA-based mass spectrometry, and data analysis by plexDIA, we aimed to demonstrate its utility to understand proteome response to cellular perturbations. Specifically, we studied the response of Hela cells to interferon gamma (IFNg) in a time-resolved manner to identify proteins that are induced by this immune-stimulatory factor. Therefore, we treated Hela cells with IFNg and collected cells at five different time points (2-24 h), each with a 0.5% (w/v) BSA-treated control, and all in 3 replicates (i.e. totalling 30 samples). Notably, cells for each sample were grown in one well in a 6-well plate which sufficed to obtain >50 µg total protein per condition. Importantly, cells were lysed and proteins extracted by AFA-ultra-sonication for all samples simultaneously in a 96-well plate [45], followed by automated NSP enrichment and peptide clean-up with automated SP3 both on a Bravo liquid handling platform. Thus, this collectively constitutes an integrated multistep workflow to process cells to purified peptides, with minimal manual intervention (Figure 5A). Upon NSP analysis by DIA mass spectrometry (90 min method, 70 min active gradient) and data

bioRxiv preprint doi: https://doi.org/10.1101/2023.03.03.530942; this version posted March 3, 2023. The copyright holder for this preprint (which was not certified by peer review) is the author/funder, who has granted bioRxiv a license to display the preprint in perpetuity. It is made available under aCC-BY-NC-ND 4.0 International license.

analysis by plexDIA, >6000 proteins were quantified per time point and replicate, overall totalling 8130 protein groups (6887 unique proteins) (Figure 5B, Supplementary Data 4). The rate of missing values remained at a moderate 18.11% across the whole data set, and on average was 9.58% for individual samples, reflecting a key merit of DIA. Precision of quantification (6-8 %, Figure 5C) was within the same range as for the benchmark data set (Figure 4D). Shorter labelling times did not lead to a noticeable reduction in the number of quantified proteins or precision (Figure 5B and C), indicating that even sparsely labelled proteins were confidently identified and quantified. Using principal component analysis (PCA), the individual replicates of the samples clustered together for each time point, following the time course of IFNg treatment, indicating a progressive and reproducible effect in the newly synthesized proteome (Figure 5D). This was confirmed in a differential protein expression analysis, where multiple significant changes in the newly synthesized proteome were detected at each time point, even as early as 2 h (Figure 5E and Supplementary Data 5. Most of the significantly upregulated proteins are known downstream targets of IFNg, or are directly involved in the IFNg signalling pathway (Figure 5F), including ICAM1, STAT1 and TAP1 which were among the earliest detected proteins, already observed after 2h and 4h (Figure 5E). Compared to published newly synthesized proteome analysis data of IFNg-treated Hela cells, prepared with the PhosID methodology [24], the QuaNPA workflow achieves greater proteome coverage and higher sensitivity in the detection of characteristic IFNg-induced protein expression changes (Supplementary figure 4). Specifically, we identified 2.5-fold more proteins from 5-fold lower protein input, and were able to identify various IFN-related gene sets at the 4h time point that were missed by PhosID at this early time point (Supplementary Figure 4), indicating the sensitivity and efficiency of the QuaNPA workflow. Furthermore, when comparing our data to previous work studying IFNg response at the transcriptome level[47], across all time points we observed a significant enrichment of proteins whose mRNA was upregulated (Supplementary Data 6, and whose gene promoters were bound by STAT1 (Figure 5F, Supplementary Data 7). Indeed, a modest positive correlation was observed between mRNA and NSP expression (R=0.43), which was increased when only considering proteins that were differentially expressed (R=0.66) or when only considering STAT1 targets (R=0.54) (Supplementary Figure 5). Notably, several differentially expressed transcripts did not lead to a change in protein expression, and conversely multiple differentially synthesized proteins had no significant change in their mRNA abundance (Supplementary Figure 5), indicating the role of translational regulation.

By combination of the data from different time points of IFNg treatment, we evaluated temporal profiles of differentially expressed NSPs. Proteins were assigned to 3 groups to classify their early (2 h), intermediate (4-9 h) or late response to IFNg (24 h), depending on the earliest time point that differential expression was observed with statistical significance (absolute log2 fold change > 1 and adj. p-value < 0.05, at any of the 5 time points and CV < 20 % across all time points; Supplementary Data 8. Furthermore, for these proteins we collected additional evidence for IFNg regulation, by listing the number of reported datasets in the interferome.org database[48] that provided evidence for their regulation by IFNg, in human cells (Figure 6). At the early time point of 2 h IFNg treatment, a small set of proteins is differentially expressed, including

bioRxiv preprint doi: https://doi.org/10.1101/2023.03.03.530942; this version posted March 3, 2023. The copyright holder for this preprint (which was not certified by peer review) is the author/funder, who has granted bioRxiv a license to display the preprint in perpetuity. It is made available under aCC-BY-NC-ND 4.0 International license.

ICAM1, SOD2 and STAT1, which is the major transcriptional mediator in the IFNg signalling pathway. These three proteins are well-established targets of IFNg signalling with numerous reports of induced expression upon IFNg stimulation, establishing them as known IFNg hallmark proteins. Additionally, strong and rapid upregulation was observed for ZC3HAV1 (PARP13), a protein with a strong anti-viral function and prominently reported in the interferome as a target of IFNg, although it is not listed as an IFNg-response gene according to GSEA-Hallmark or gene ontology data (Figure 6). Interestingly, differential expression of the adapter protein TICAM1 was only detected at the 2 h and has only been mentioned in very few reports in relation to IFNg, making it a potential novel or at least under-studied candidate as an IFNg-responsive protein. Proteins with differential expression 4-9 h after IFNg stimulation also included multiple well-characterised targets of IFNg, such as endogenous peptide antigen transporter TAP1, its interaction partner TAPBP and TAP2, MHC class-I component HLA-E, tryptophan tRNA-ligase WARS1, transcription factor SP110 and phospholipid scramblase PLSCR1. The group of proteins that showed a delayed response to IFNg (24h) primarily consists of proteins associated with functions of the immune system. Complement proteins C1S and C3 and proteins involved in endogenous antigen presentation via MHC class I, including HLA-A, HLA-C, HLA-H, PSME1. In addition, other hallmark proteins of IFNg response were found in this category, such as IFIH1, IFI30, PML, and PARP12, reaching maximum levels late (24h) after IFNg treatment, although for nearly all of them expression gradually increased for the duration of IFNg exposure (Figure 6). Beyond this, we identified differential expression of several more proteins which have not been previously reported as IFNg targets, such as KLF3 and SIN3B (Figure 6, Supplementary Table 5). Interestingly, both these transcription factors have established roles in hematopoiesis[49 50], with prior evidence of being regulated by IFNg[51 52], despite not being listed in interferome.org. These data show that QuaNPA identifies bona fide targets of IFNg, in line with IFNg's known role to induce hematopoiesis.

Apart from proteins whose expression is induced by IFNg, we observed a smaller group that are repressed, such as of CXCR4 (Fusin) and IER3 (Figure 6). IFNg-induced downregulation of CXCR4 was previously shown to result in reduced tumor metastasis and virus replication [53]. In addition, we observed reduced synthesis of several proteins that to the best of our knowledge have not been reported as IFNg responsive proteins, including stark and immediate (2h) downregulation of the mitochondrial protein MT-ATP8, and more gradual decrease of BICD2, S100A6 and SUMO1. Interestingly, these latter three proteins have previously been shown to negatively regulate STAT1 signalling: depletion of BICD2 was shown to increase levels of STAT1 mRNA[54], S100A6-knockdown lead to increased protein levels and phosphorylation of STAT1[55], and SUMO1-conjugation of STAT1 lead to reduced levels of STAT1 phosphorylation and transcription of IFNg response genes[56]. Therefore, our data indicates that IFNg-induced downregulation of these targets constitutes a feed-forward mechanism to enhance IFNg signalling output.

Collectively, the QuaNPA workflow allowed us to quantify proteome-wide changes in protein synthesis in response to IFNg in a time-resolved manner, benefitting from automated sample preparation and reduced

bioRxiv preprint doi: https://doi.org/10.1101/2023.03.03.530942; this version posted March 3, 2023. The copyright holder for this preprint (which was not certified by peer review) is the author/funder, who has granted bioRxiv a license to display the preprint in perpetuity. It is made available under aCC-BY-NC-ND 4.0 International license.

input requirements. We detected changes in the newly synthesized proteome at various time points during the time course of IFNg treatment, distinguishing immediate and delayed events occurring at 2h or gradually towards 24h, indicating primary and secondary targets of IFNg signalling. Importantly, this included induction or repression of established IFNg target proteins as well as many novel ones, demonstrating the power of QuaNPA to infer novel biology from temporal expression profiling of newly synthesized proteins.

Discussion

The analysis of newly synthesised proteins affords distinct conceptual advantages over conventional protein abundance profiling, giving insight in the cell's proteome response to perturbations at rapid time scales. Yet, involved protocols for labelling of cells, enrichment of NSPs, and analysis of data result in a labor-intensive methodology with low throughput and sensitivity, thus hampering adoption in the field. In QuaNPA, we have addressed these issues while maintaining the benefits of AHA-labelling, protein enrichment, and pulsed SILAC labelling. We have achieved this by designing novel high-capacity alkyne-functionalized magnetic sepharose beads, by automating protein enrichment, by implementing a single-shot DIA-based LCMS methodology, and by using DIA-NN's plexDIA-function for data analysis. Moreover, we integrated this with the autoSP3 protocol that we developed recently [45], combining multiplexed cell lysis by AFA-based sonication and protein/peptide clean-up by SP3 on the same Bravo liquid handling platform used for NSP enrichment. Collectively, QuaNPA thus constitutes an integrated pipeline with minimal manual intervention, and processing of samples in the same plate throughout. As a result, the semi-automated enrichment of 96 samples is completed in 5.5 h for 96 samples (4.25 h for 8 samples), including the 2h-incubation of the CuAAC-based coupling of the NSPs to the magnetic alkyne beads, and subsequent washing steps that make up most of the protocol runtime. Tryptic digestion of the samples was carried out off the Bravo deck since it requires a heated lid. Lyophilization of the diluted tryptic peptides can be carried out in approximately 1.5 h, and subsequent peptide purification via autoSP3 takes about 1.25 h of runtime, all for 96 samples simultaneously. QuaNPA requires low amounts of input material (≤ 100 µg) to obtain high quality data (Figure 3E, 3F, S4), which enables the use of small culturing flasks/dishes such as 6-well plates, thus rendering large-scale studies with multiple cellular treatments a manageable endeavour.

When evaluating QuaNPA using a pulsed-SILAC and AHA-labelled HeLa sample, we found that protein enrichment on MAA beads modestly increased the total number of identified NSPs compared to omission of enrichment (Figure 3B), which is in line with our previous observations [5]. More importantly, enrichment of NSPs improved the quantification of newly synthesized proteome analysis (Figure 3C and 3D). Both observations can be readily explained by the removal of the excess of pre-existing proteins, increasing the signal-to-noise of peptides originating from AHA-containing proteins. Through usage of the MAA beads in a semi-automated protocol, efficiency of NSP enrichment was maintained across a broad range of protein input amounts (1-300 µg, Fig 3E), enabling diverse study designs both with low or non-limited cell numbers.

bioRxiv preprint doi: https://doi.org/10.1101/2023.03.03.530942; this version posted March 3, 2023. The copyright holder for this preprint (which was not certified by peer review) is the author/funder, who has granted bioRxiv a license to display the preprint in perpetuity. It is made available under aCC-BY-NC-ND 4.0 International license.

As observed in this study, even stringent washing steps during NSP enrichment cannot completely remove unlabelled pre-existing proteins. These can be readily recognized by their SILAC labelling status, contrasting with label-free approaches [15,24,57,58] where such contaminants cannot be distinguished from genuine NSPs, thereby compromising quantitative accuracy.

The recently developed plexDIA functions of DIA-NN enables the DIA-based analysis of multiplexed samples with non-isobaric labels[44]. Since analysis of label-free samples via DIA has been demonstrated to achieve deep proteome coverage in single LC-MS runs (i.e. without peptide fractionation), similar performance for SILAC-labelled proteins would save measurement time, and increase throughput of the QuaNPA workflow. Indeed, we observed a major increase in the number of identified proteins in our benchmark sample when using either of the tested DIA methods, doubling the number to 6000 proteins compared to DDA analysis (Figure 4C). Accordingly, very similar numbers were achieved when analysing the actual NSP samples in the time course analysis of IFNg treatment (Figure 5B). These results were obtained without optimization of other parameters in DIA-NN. In particular, and in contrast to conventional DDA SILAC search engines, DIA-NN does not feature a “re-quantify” function, which enables the calculation of SILAC ratios with labelled peptides whose intensity is close to noise level. Instead, DIA-NN calculates channel and peak translation q-values, which at high stringency lead to filtering of labelled peptide ions with very low intensity. Our benchmark showed that plexDIA performed particularly well for triple-SILAC samples that resemble enriched NSPs. In addition, we observed high quantitative accuracy and precision when using plexDIA both with MS1- and MS2-optimized quantification, showing comparable performance to conventional DDA analysis. (Figure 4D, E). Since we obtained high quality data with stringent translated- and channel q-value filters, we did not extensively investigate the different features of the DIA-NN output tables such as the multiple quantitative metrics and q-value filters. Optimization of these parameters might further improve proteomic depth and quantitative accuracy of samples with large SILAC ratios, as in our mix1. In recent work using different instruments for plexDIA, such as the timsTOF SCP, MS1-based quantification was preferred over MS2-based quantification [44,59]. This somewhat contrasts with our observations (Figure 4), however this may result from the use of a different mass spectrometer, from the use of low-input samples at the single cell level, and from the fact that samples were labelled using different methods. Future work should further delineate the best approach for diverse use cases, but nevertheless these published data, now augmented with our SILAC data, demonstrate that non-isobaric labelling can be effectively used in DIA-based workflows for multiplexed proteomic experiments. The capacity to analyse NSP samples in single LC-MS runs has important implications, since it enhances throughput by significantly reducing measurement times. These characteristics make that the QuaNPA workflow is ideally placed for quantitative NSP analyses across multiple conditions, such as different cellular treatments or time course experiments.

We applied QuaNPA to investigate cellular response of HeLa cells to IFNg, since this is a well-characterized perturbation with many known targets to allow benchmarking of our data. For instance, the biological system

bioRxiv preprint doi: https://doi.org/10.1101/2023.03.03.530942; this version posted March 3, 2023. The copyright holder for this preprint (which was not certified by peer review) is the author/funder, who has granted bioRxiv a license to display the preprint in perpetuity. It is made available under aCC-BY-NC-ND 4.0 International license.

has also been used in global proteome and transcriptome analysis, and in two recent strategies coupling AHA-containing NSPs to phosphonate alkynes[24] or biotin-alkyne[60] with subsequent affinity purification via an Bravo AssayMap platform. However, both protocols require relatively large amounts of protein input (500 µg per sample/condition[24], i.e. 10x more than in QuaNPA), or lysates form cells grown in 15 cm dishes[60] , and they contain long additional steps, such as overnight dephosphorylation [24] or dialysis [60], likely leading to protein losses and contributing to the reduced proteomic depth and sensitivity compared to QuaNPA (Supplemetary figure 4). In our data we observed the upregulation of multiple well-established downstream targets of IFNg signalling. Importantly, core response proteins (ICAM1, STAT1, SOD2) were already observed after 2h of IFNg treatment, i.e. much earlier than in previous work [24,60]. In addition, many other IFNg-targets exhibited a gradual increase in protein synthesis over time, including known as well as novel proteins for which we could not find prior association with IFNg signalling [48]. We anticipate that proteins observed to be immediately regulated (2-4 h) may be direct targets of IFNg, including those that go down in expression such as SUMO1, S100A6 and MT-ATP8 (Figure 6). Others may also represent secondary responses, regulated by the large number of IFNg hallmark proteins induced during the time course. Detailed experiments will be needed to distinguish these possibilities, and to functionally validate their role in the IFNg signalling network.

In conclusion, the QuaNPA workflow features automated sample preparation of up to 96 samples in parallel, enabling the detection of changes in protein synthesis with high quantitative accuracy and precision with increased proteome coverage, while requiring short metabolic labelling and LC-MS/MS measurement times. Although we used AHA here as a mark for protein NSP enrichment, it is readily conceivable to implement other clickable amino acids or puromycin analogues in the workflow. In addition, performance characteristics of QuaNPA should enable combined studies with global protein expression profiling, to benefit from complementary insights that can be gained from alterations in protein synthesis and in overall protein abundance. We anticipate that QuaNPA will empower large-scale NSP analyses in numerous biological contexts to understand the proteomic response that is elicited by diverse perturbations and signalling events.

Material and Methods

Preparation of magnetic alkyne agarose beads

Epoxy-activated magnetic agarose beads (Cube Biotech) were coupled with propargylamine (Santa Cruz Biotechnology) to produce magnetic alkyne agarose (MAA) beads. 5 mL epoxy-activated magnetic agarose beads were washed with 10 mL milliQ water and resuspended in the coupling solution of 1 M propargylamine in 0.5 M dipotassium phosphate solution (pH 10.5). The handling of the propargylamine and coupling solution were carried out under a fume hood with appropriate safety precautions. The beads and coupling solution were incubated in a thermo shaker at 45 °C for 16 h, and beads were then washed

bioRxiv preprint doi: https://doi.org/10.1101/2023.03.03.530942; this version posted March 3, 2023. The copyright holder for this preprint (which was not certified by peer review) is the author/funder, who has granted bioRxiv a license to display the preprint in perpetuity. It is made available under aCC-BY-NC-ND 4.0 International license.

with 25 mL milliQ water. To ensure the complete quenching of remaining epoxy groups on the beads, they were incubated with 1 M Tris-HCl buffer (pH 8.0) for 4 h. The beads were subsequently washed with 45 mL milliQ water and stored in 20 mM sodium acetate buffer (pH 6.5) with 20 % ethanol at 4 °C. The MAA beads are stable at 4 °C for multiple months.

Cell culture

Hela cells were grown in DMEM high glucose medium (Gibco) supplemented with 2 mM L-glutamine, 10 % (v/v) fetal bovine serum (Gibco) and additional 2 mM GlutaMAX (Gibco). For the interferon gamma (IFNg) stimulation experiments, Hela cells were treated with 10 ng/mL recombinant IFNg (Cell signalling), diluted in 0.5 % (w/v) bovine serum albumin (Serva). For the preparation of the SILAC benchmark samples, Hela cells were grown in high glucose DMEM, with the previously listed supplements, and heavy- ($^{13}C_6{}^{15}N_4$-Arg, $^{13}C_6{}^{15}N_2$-Lys), intermediate ($^{13}C_6$-Arg, D_4-Lys) or light isotope-containing Lysine, Arginine for 10 days. Hela cells were grown in 15-cm dishes for the preparation of newly synthesized proteome samples used for protocol optimization. For the SILAC benchmark sample preparation, the cells were grown in 10-cm dishes and for the preparation of the newly synthesized proteome samples of IFNg treated Hela cells the cells were grown in 6-well plates.

Metabolic labelling of newly synthesized proteins

A metabolic labelling approach, combining pulsed stable isotope-labelling (pSILAC) and L-Azidohomoalanine (AHA)-based labelling of newly synthesized proteins was used. Prior to the labelling, the cells were washed with warm PBS and incubated with DMEM high glucose medium deprived of Methionine, Arginine and Lysine for 45 min. The pulsed SILAC and AHA labelling was carried out with Methionine-free DMEM high glucose medium containing heavy- ($^{13}C_6{}^{15}N_4$-Arg, $^{13}C_6{}^{15}N_2$-Lys) or intermediate ($^{13}C_6$-Arg, D_4-Lys) Lysine, Arginine and 100 µM AHA for 2 h, 4 h or for a maximum of 6 h. The cells used for initial method optimization were labelled for 4 h without any perturbations. The IFNg-stimulated cells were labelled for the indicated IFNg treatment time, except for the 9h and 24 h timepoints, in which the cells were labelled during the last 6 h of IFNg exposure.

Cell lysis and ultrasound sonication

Cells were lysed with lysis buffer containing 1% Sodium-dodecylsulfate (SDS), 300 mM HEPES (pH 8.0) and cOmplete EDTA-free protease inhibitor cocktail (Merck). Lysates, which were used for the method optimization and SILAC benchmark were sonicated with a probe sonicator (Branson) at 10% power for 1 min. The IFNg-treated cells were sonicated in AFA-tube TPX strips (Covaris), using a Covaris LE220R-Plus for 300 s at 325 peak power with a duty factor of 50 %, 200 cycles per burst, average power of 162.5. The dithering parameters were set to ± 5 mm in x and z direction and 4.5 mm in y direction at a speed of 20 mm/s. Protein concentrations of the sonicated lysates were determined using a BCA assay (Pierce). A

bioRxiv preprint doi: https://doi.org/10.1101/2023.03.03.530942; this version posted March 3, 2023. The copyright holder for this preprint (which was not certified by peer review) is the author/funder, who has granted bioRxiv a license to display the preprint in perpetuity. It is made available under aCC-BY-NC-ND 4.0 International license.

total of 100 µg (50 µg per condition) protein was used as input for the enrichments, except in dilution series to test performance at lower input.

Automated enrichment of newly synthesized proteins

The automated newly synthesized proteome enrichment protocol was programmed to enable the processing of up to 96 samples in parallel in a PCR plate. By setting the number of columns on the sample plate, incubation times, volumes of buffers and reagents as variables, adaptations to the protocol can easily be introduced.

The combined lysates were diluted to a total volume 150 µL using lysis buffer. In order to prevent the coupling of proteins containing strongly nucleophilic Cysteine to the beads [61], the samples were alkylated by addition 3.4 µL of 600 mM iodoacetamide (IAA) for 20 min at room temperature. Subsequently, 20 µL of magnetic alkyne agarose (MAA) beads, diluted in lysis buffer and the Copper(I)-catalyzed Azide Alkyne Cycloaddition (CuAAC) reaction[62,63] mixture were added, containing 21.62 mM $CuSO_4$, 108.11 mM Tris-hydroxypropyltriazolylmethylamine (THPTA), 216.22 mM pimagedine hydrochloride and 216.22 mM sodium ascorbate. Next, the plate was removed from the Bravo platform, sealed using VersiCap Mat 96-well flat cap strips (Thermo Fischer Scientific) and incubated for 2 h at 40 °C in a thermal shaker. Following the coupling of the AHA-containing newly synthesized proteins (NSP), the plate was unsealed and moved back onto the orbital shaker (position 9, Supplementary Figure 1) on the Bravo platform, and the supernatant was removed, by placing the sample plate on a magnetic rack (ALPAQUA MAGNUM FLX enhanced universal magnet) for 30 s and aspirating the supernatant in two steps using tips from position 6 and dispensed in the waste plate (position 2). The beads were subsequently washed with 150 µL milliQ water. After addition of the liquid to the beads on the orbital shaker, the plate was moved to the heating station (position 4) where the beads were mixed by pipetting up and down 8 times with a constant flow rate of 300 µL/s, to prevent aggregation of the beads. Next, the plate was transferred onto the magnetic rack and the supernatant was removed. The NSP bound to the beads were subsequently reduced and alkylated by addition of 150 µL of 10 mM Tris(2-carboxylethyl)phosphine (TCEP) and 40 mM 2-chloroacetaminde (CAA), dissolved in 100 mM Tris-HCl buffer (pH 8.0), containing 200 mM NaCl, 0.8 mM Ethylendiamintetraacetic acid (EDTA), 0.8% SDS and incubating on the heating station at 70 °C for 20 min and subsequent incubation at 20 °C for 15 min on the orbital shaker. The beads were subsequently washed three times with 1% SDS dissolved in 100 mM Tris-HCl (pH 8.0), 250 mM NaCl and 1 mM EDTA buffer, once with milliQ H_2O, three times with 6 M Guanidine-HCl in 100 mM Tris-HCl (pH 8.0) and three times with 70% ethanol, in consecutive washing steps of 150 µL each. Following the washing steps, the beads were resuspended in 50 µL 100 mM Ammonium bicarbonate buffer (pH 8.0). Proteins were digested off the beads by adding 6 µL of 1 µg/µL sequencing grade Trypsin (Promega), diluted in 50 mM acetic acid, for 16 h at 37 °C, which was performed in a thermal shaker after sealing the plate with VersiCap Mat 96-well flat cap strips.

bioRxiv preprint doi: https://doi.org/10.1101/2023.03.03.530942; this version posted March 3, 2023. The copyright holder for this preprint (which was not certified by peer review) is the author/funder, who has granted bioRxiv a license to display the preprint in perpetuity. It is made available under aCC-BY-NC-ND 4.0 International license.

Automated peptide purification

The automated SP3 protocol was used for the purification of peptides by processing of 16-96 samples in parallel on a Bravo liquid handling robot [45]. Following protein digestion, the peptide-containing supernatant was transferred from the sample plate on position 7 onto a new plate on position 8, and peptides were lyophilized using a UNIVAPO-150H vacuum concentrator, coupled to a UNICRYO MC2 cooling trap and UNITHERM 4/14 D closed circuit cooler (UNIEQUIP). On the Bravo platform, magnetic carboxylate Sera-Mag Speed Beads (Fischer Scientific) were diluted to 100 µg/µL in 10 % formic acid and 5 µL were added to each lyophilized sample. Aggregation of the peptides onto beads was induced via addition of 195 µL acetonitrile and incubating for 18 min, while shaking at 100 rpm on the orbital shaker. Next, the supernatant was removed from the magnetic rack in two steps. The beads were washed 2 times with 180 µL acetonitrile and subsequently dried. In the final steps the beads were resuspended in 20 µL 0.1 % formic acid in water and sonicated in an Ultrasonic Cleaner USC-T (VWR) for 10 min and the supernatant was transferred to a new plate. The purified peptides were dissolved in 0.1 % formic acid and used for LC-MS/MS analysis.

Preparation global proteome samples for pulse-labelling input and SILAC benchmark samples

50 µg of AHA and SILAC pulse-labelled Hela cell lysate and 100 µg of 10 day-long SILAC-labelled cell lysate were used for the preparation of global proteome samples, which were used to compare non-enriched and enriched NSP samples and to evaluate different mass spectrometry acquisition methods. Cells were lysed with 1% SDS and 300 mM HEPES (pH 8.0) containing lysis buffer, sonicated with a probe sonicator (Branson) for a total of 1 min per lysate. The protein concentration of the lysates was determined using a BCA assay (Pierce) and the lysates of the labelled Hela cells were combined with 2 defined ratios, to a total of 100 µg protein input. The 2 different SILAC mix samples were created to represent an enriched newly synthesized proteome sample and a pulse-labeled sample without enrichment. The mix 1 sample consisted of 70 % unlabeled protein, 15 % heavy and 15% intermediate SILAC labeled protein, whereas the mix 2 sample consisted of 40 % heavy, 40 % intermediate labeled protein and 20 % unlabeled protein. Proteome samples of the labelled lysates were prepared using the SP3 protein and peptide purification protocol as previously described [64].

LC-MS/MS

Quantitative measurements of tryptic peptides, of the enriched newly synthesized proteins and global proteome, was carried out using an EASY-nLC 1200 system (Thermo Fischer Scientific) coupled to a QExactive HF mass spectrometer (Thermo Fischer Scientific).

The peptides were separated by reverse-phase liquid chromatography using 0.1 % formic acid (solvent A) and 80 % acetonitrile (solvent B) as mobile phases. Peptide separation occurred on an Acclaim PepMap trap column (Thermo Fisher Scientific, C18, 20 mm × 100 µm, 5 µm C18 particles, 100 Å pore size) and a nanoEase M/Z peptide BEH C18 analytical column (Waters, 250 mm × 75 µm 1/PK, 130 Å, 1.7 µm). The

bioRxiv preprint doi: https://doi.org/10.1101/2023.03.03.530942; this version posted March 3, 2023. The copyright holder for this preprint (which was not certified by peer review) is the author/funder, who has granted bioRxiv a license to display the preprint in perpetuity. It is made available under aCC-BY-NC-ND 4.0 International license.

samples were loaded onto the trap column with constant flow of solvent A at a maximum pressure of 800 bar. The analytical column was equilibrated with 2 µL solvent A at a maximum pressure of 600 bar heated to 55 °C using a HotSleeve+ column oven (Analytical SALES & SERVICES). The peptides were eluted with a constant flow rate of 300 nL/min. Concentration of solvent B was gradually increased during the elution of the peptides in either of three different HPLC gradients used in this study.

The gradient used for the analysis of the newly synthesized proteome and input samples started with 4 % solvent B and was increased to 6 % in the first 1 min, increased to 27 % at 70 min and further increased to 44 % after 85 min. After 85 min the percentage of solvent B was raised to 95 %. After 95 min the system was re-equilibrated using 5 % solvent B for 10 min. The gradient used for the analysis of the SILAC labelled Hela benchmark samples started with 3 % solvent B for the first 4 min, increased to 8 % after 4 min and to 10 % after 6 min. After 68 min the percentage of solvent B was raised to 32 % and after 86 min to 50 %. From 87 min till 94 min of the gradient the percentage of solvent B increased to 100 %. After 95 min the system was re-equilibrated using 3 % solvent B for 10 min. The gradient used for the analysis of the newly synthesized proteome samples of IFNg treated Hela cells started with 4 % solvent B and was increased to 6 % in the first 1 min, increased to 27 % at 51 min and further increased to 44 % after 70 min. After 70 min the percentage of solvent B was raised to 95 %. After 80 min the system was re-equilibrated using 5 % solvent B for 10 min. Eluting peptides were ionized and injected into the mass spectrometer, using the Nanospray flex ion source (Thermo Fischer Scientific) and a Sharp Singularity nESI emitter (ID = 20 µm, OD = 365 µm, L = 7 cm, α = 7.5°) (FOSSILIONTECH), connected to a SIMPLE LINK UNO-32 (FOSSILIONTECH). A static spray voltage of 2.5 kV was applied to the emitter and the capillary temperature of the ion transfer tube was set to 275 °C.

The QExactive HF mass spectrometer was operated in the data-dependent (DDA) or data-independent (DIA) mode for the five different acquisition methods evaluated in this study. Detailed descriptions of the different HPLC- and mass spectrometry methods can be found in the supplementary material. DDA methods for the measurements of the NSP samples, input samples and SILAC-labelled Hela samples only differed in their HPLC gradient. In all cases, a full scan range of 375-1500 m/z, Orbitrap resolution of 60000 FWHM, automatic gain control (AGC) target of 3e6 and maximum injection time of 32 ms was set and data-dependent MSMS spectra were acquired using a Top 20 scheme, using a fixed scan range from 200-2000 m/z and fixed first mass of 110 m/z. The quadrupole isolation window was set to 2.0 m/z and normalized collision energy was set to 26. The Orbitrap resolution was set to 15000 FWHM with an AGC target of 1e5 and maximum injection time of 50 ms. MSMS spectra were acquired in profile mode and a charge state exclusion of 1, 5-8 & >8 was defined. An intensity threshold of 2e4 and a minimum AGC target of 1e3 was set.

Two different DIA methods were used for the analysis of the SILAC-labelled Hela benchmark samples. In DIA method 1 a full scan range of 400-1000 m/z with Orbitrap resolution of 60000 FWHM, 3e6 AGC target and maximum injection time of 20 ms was set. Data-independent MSMS spectra were acquired with an Orbitrap resolution of 30000 FWHM, maximum injection time of 50 ms and AGC target of 1e6, using 26

bioRxiv preprint doi: https://doi.org/10.1101/2023.03.03.530942; this version posted March 3, 2023. The copyright holder for this preprint (which was not certified by peer review) is the author/funder, who has granted bioRxiv a license to display the preprint in perpetuity. It is made available under aCC-BY-NC-ND 4.0 International license.

equally sized, 1 Th overlapping isolation windows with a width of 23.3 m/z. The normalized collision energy for the fragmentation of precursor ions was set to 27 and a fixed first mass of 200 m/z was set for the acquisition of the MSMS spectra. DIA method 2 used three full scans with a range from 400-1000 m/z, Orbitrap resolution of 120000 FWHM, 3e6 AGC target and maximum injection time of 20 ms. Data-independent MSMS spectra were acquired with an Orbitrap resolution of 30000 FWHM, maximum injection time of 50 ms and AGC target of 1e6, using 27 equally sized, 1 Th overlapping isolation windows with a width of 23.2 m/z. The normalized collision energy for the fragmentation of precursor ions was set to 27 and a fixed first mass of 200 m/z was set for the acquisition of the MSMS spectra. For the analysis of the IFNg-treated NSP samples, a different DIA method was used. This third DIA method featured a full scan range of 400-1000 m/z, Orbitrap resolution of 60000 FWHM, 3e6 AGC target and maximum injection time of 40 ms. Data-independent MSMS spectra were acquired with an Orbitrap resolution of 30000 FWHM, maximum injection time of 40 ms and AGC target of 1e6, using 28 equally sized, 1 Th overlapping isolation windows with a width of 22.0 m/z. The normalized collision energy for the fragmentation of precursor ions was set to 27 and a fixed first mass of 200 m/z was set for the acquisition of the MSMS spectra. Detailed summaries of the LC-MS methods used in this study can be found in the supplementary material.

Data analysis

Raw files from DDA measurements were processed using Maxquant version 2.0.3 and the Andromeda search engine [65], using a human proteome fasta file, retrieved from the SwissProt database (version from February 2021 with 20934 entries). The enzymatic digestion was set to Trypsin/P and a maximum of 2 missed cleavages per peptide were allowed. For the analysis of NSP data, raw files of both the NSP and global proteome samples were processed together, using Maxquant version 2.0.3. The multiplicity was set to 3, comprising of a light channel, an intermediate channel with Arg6 and Lys4 and heavy channel with Arg10 and Lys8. Cysteine carbamidomethylation was set as fixed modification, whereas Methionine oxidation, N-terminal acetylation, and deamidation of Asparagine and Glutamine were set as variable peptide modifications. The Re-quantify function was enabled, match-between-runs was disabled and other search functions were left with default parameters. Only for the analysis of the SILAC labelled Hela benchmark samples, the match-between-runs function was enabled. Unique and razor peptides were used for quantification and normalized SILAC ratios and iBAQ values were calculated. The minimum ratio count was set to 0 to not exclude identifications in single SILAC channels. The PSM and protein FDR threshold was set to 1%.

Raw files from DIA measurements were analysed using DIA-NN [46] version 1.8.1. A predicted spectral library was generated from the fasta file, which was also used in the Maxquant searches. Additionally, a fasta file containing common protein contaminants was added for the spectral library prediction [66]. Default settings were used for the spectral library prediction, with the addition of Methionine oxidation as variable modification. For the processing of the raw files, the default settings of DIA-NN were used with additional functions from the plexDIA module enabled [44]. Three SILAC channels with mass shifts corresponding to

bioRxiv preprint doi: https://doi.org/10.1101/2023.03.03.530942; this version posted March 3, 2023. The copyright holder for this preprint (which was not certified by peer review) is the author/funder, who has granted bioRxiv a license to display the preprint in perpetuity. It is made available under aCC-BY-NC-ND 4.0 International license.

Lys, Lys4 (+4.025107 Da), Lys8 (+8.014199 Da), Arg, Arg6 (+6.020129 Da), Arg10 (+10.008269 Da) and an additional decoy channel with Lysine (+12.0033 Da) and Arginine (+13.9964 Da) were registered. Translation of retention times between peptides within the same elution group was enabled. The first ^{13}C-isotopic peak and monoisotopic peak was included for the quantification and the MS1 deconvolution level was set to 2. Precursor matrix output tables were filtered for FDR < 0.01 and additionally for channel q-value < 0.01 and translated q-value < 0.01. The MBR function was enabled to increase data completeness. The output tables from Maxquant ("ProteinGroups.txt", "evidence.txt") and DIA-NN ("report.pr_matrix_channels_translated.tsv" and "report.pr_matrix_channels_ms1_translated.tsv") were processed in the R software environment (version 4.0.3) using custom scripts. Identified contaminants were removed and protein abundance was calculated using the MaxLFQ algorithm, applied to the individual SILAC channels, using the iq R-package function "process_long_format()" [67]. For MS1- and MS2-based quantification, the "Ms1.translated" and "precursor.translated" quantity was used for the MaxLFQ calculation, respectively. Protein-group SILAC ratios were calculated for each sample using the LFQ values. For the analysis of the IFNg-treated Hela cells, only MS2-based quantification was used. Principle component analysis (PCA) of the log2 transformed SILAC ratios was performed using the "prcomp" function of the stats R-package. Peptide hydrophobicity (GRAVY index) was calculated using the "hydrophobicity" function of the Peptides R package. For differential expression analysis, only unique protein groups (single Uniprot identifier) with a minimum of 2 SILAC ratios values in 3 replicates were used. Differential expression tests were carried out using the Limma [68] and DEqMS [69] R/Bioconductor packages, by fitting the data onto a linear model and performing an empirical Bayes moderated t-test. The number of precursors, with consideration of modified peptide sequences and charge but not SILAC channels, of each protein group was included as a factor for the variance estimation in DEqMS. Overrepresentation enrichment analysis of significantly deregulated protein groups (absolute log2 fold change > 0.585 and adjusted p-value < 0.05), from the IFNg time course experiments, was carried out using the "enricher" function of the clusterProfiler [70] R/Bioconductor package. Gene set enrichment analysis was carried out using the sorted log2 fold change values of all quantified protein groups, using the "GSEA" and "gseGO" function of the clusterProfiler [70] R/Bioconductor package. Gene lists of the Molecular Signatures Database were retrieved and analysed using the msigdbr package of the CRAN software repository [71]. Gene sets of the Hallmark (H) subset were included in the analysis. Additionally, the top 500 significantly upregulated genes from the 24 h IFNg-treated Hela cells of the deposited RNA-seq dataset (GSE150196, more specifically "GSE150196_RNA-seq_DESeq2_priming_vs_naive.tab") [47] and the top 500 target genes from a public STAT1 ChIP-seq dataset from 30 min IFNg treated Hela S3 cells (ENCSR000EZK, more specifically "ENCFF039MZH.bed") were included in the enrichment analysis [72]. The ChIP-seq data was processed using a custom R-script, only genes within 2000 bp upstream or downstream of the annotated transcription start sites of the hg38 reference genome were included in the final STAT1 target gene list. Quantified protein groups in the respective condition were included as background gene list for the enrichment and p-values were adjusted using the Benjamini-Hochberg approach[73]. The number of datasets in which differential expression of

bioRxiv preprint doi: https://doi.org/10.1101/2023.03.03.530942; this version posted March 3, 2023. The copyright holder for this preprint (which was not certified by peer review) is the author/funder, who has granted bioRxiv a license to display the preprint in perpetuity. It is made available under aCC-BY-NC-ND 4.0 International license.

643 selected proteins or genes was reported in response to IFNg in human cells or tissues, was retrieved from
644 the interferome.org database [48].
645
646

bioRxiv preprint doi: https://doi.org/10.1101/2023.03.03.530942; this version posted March 3, 2023. The copyright holder for this preprint (which was not certified by peer review) is the author/funder, who has granted bioRxiv a license to display the preprint in perpetuity. It is made available under aCC-BY-NC-ND 4.0 International license.

Data availability

The mass spectrometry data and processing parameters for the Maxquant and DIA-NN search engines have been deposited to the ProteomeXchange Consortium via the PRIDE partner repository [74]. The data from the initial method optimizations are available with identifier PXD036886, data from the SILAC labelled benchmark samples with identifier PXD039580 and PXD039578, and data from the IFNg time course experiment with identifier PXD038915. Raw MS files and the automated NSP enrichment protocol will be made available for public access upon manuscript acceptance.

Code availability

R scripts for the processing of DIA-NN and Maxquant output tables and analysis of the proteomic data in this study are available from: https://github.com/krijgsveld-lab/QuaNPA

Acknowledgements

The authors would like to thank Dr. Vadim Demichev for helpful comments and suggestions regarding the analysis of SILAC-labelled samples with DIA-NN. This work was funded in part by the German Ministry of Education and Research (BMBF), as part of the National Research Node “Mass spectrometry in Systems Medicine” (MSCoreSys), under grant agreement 161L0212A.

Author contributions

T.B. and J.K. conceived the study and designed the approach. T.B. developed the protocol for the preparation of magnetic alkyne agarose beads. T.B. prepared samples, acquired and analysed data. T.M. and T.B. created the automated enrichment protocol. J.K. together with T.B. wrote the manuscript.

Conflicts of interest

The authors declare no conflicts of interest.

bioRxiv preprint doi: https://doi.org/10.1101/2023.03.03.530942; this version posted March 3, 2023. The copyright holder for this preprint (which was not certified by peer review) is the author/funder, who has granted bioRxiv a license to display the preprint in perpetuity. It is made available under aCC-BY-NC-ND 4.0 International license.

References

1. Schwanhäusser, B. *et al.* Global quantification of mammalian gene expression control. *Nature* **473**, 337–342 (2011).

2. Buccitelli, C. & Selbach, M. mRNAs, proteins and the emerging principles of gene expression control. *Nat. Rev. Genet.* **21**, 630–644 (2020).

3. Fabbri, L., Chakraborty, A., Robert, C. & Vagner, S. The plasticity of mRNA translation during cancer progression and therapy resistance. *Nat. Rev. Cancer* **21**, 558–577 (2021).

4. Sriram, A., Bohlen, J. & Teleman, A. A. Translation acrobatics: how cancer cells exploit alternate modes of translational initiation. *EMBO Rep.* **19**, (2018).

5. Eichelbaum, K. & Krijgsveld, J. Rapid temporal dynamics of transcription, protein synthesis, and secretion during macrophage activation. *Mol. Cell. Proteomics* **13**, 792–810 (2014).

6. Ingolia, N. T., Hussmann, J. A. & Weissman, J. S. Ribosome profiling: Global views of translation. *Cold Spring Harb. Perspect. Biol.* **11**, 1–20 (2019).

7. Chothani, S. *et al.* deltaTE: Detection of Translationally Regulated Genes by Integrative Analysis of Ribo-seq and RNA-seq Data. *Curr. Protoc. Mol. Biol.* **129**, (2019).

8. Chothani, S. P. *et al.* A high-resolution map of human RNA translation. *Mol. Cell* **82**, 2885-2899.e8 (2022).

9. Liu, T. Y. *et al.* Time-Resolved Proteomics Extends Ribosome Profiling-Based Measurements of Protein Synthesis Dynamics. *Cell Syst.* **4**, 636-644.e9 (2017).

10. Ross, A. B., Langer, J. D. & Jovanovic, M. Proteome turnover in the spotlight: Approaches, applications, and perspectives. *Mol. Cell. Proteomics* **20**, 100016 (2021).

11. Ma, Y. & Yates, J. R. Proteomics and pulse azidohomoalanine labeling of newly synthesized proteins: what are the potential applications? *Expert Rev. Proteomics* **15**, 545–554 (2018).

12. Bergen, W. Van, Heck, A. J. R. & Baggelaar, M. P. Recent advancements in mass spectrometry – based tools to investigate newly synthesized proteins. *Curr. Opin. Chem. Biol.* 1–9 (2021). doi:10.1016/j.cbpa.2021.07.001

13. Iwasaki, S. & Ingolia, N. T. The Growing Toolbox for Protein Synthesis Studies. *Trends Biochem. Sci.* **42**, 612–624 (2017).

14. Aviner, R., Geiger, T. & Elroy-Stein, O. Novel proteomic approach (PUNCH-P) reveals cell cycle-specific fluctuations in mRNA translation. *Genes Dev.* **27**, 1834–1844 (2013).

15. Forester, C. M. *et al.* Revealing nascent proteomics in signaling pathways and cell differentiation. *Proc. Natl. Acad. Sci. U. S. A.* **115**, 2353–2358 (2018).

16. Barrett, R. M., Liu, H. W., Jin, H., Goodman, R. H. & Cohen, M. S. Cell-specific Profiling of Nascent Proteomes Using Orthogonal Enzyme-mediated Puromycin Incorporation. *ACS Chem. Biol.* **11**, 1532–1536 (2016).

17. Uchiyama, J., Ishihama, Y. & Imami, K. Quantitative nascent proteome profiling by dual-pulse labelling with O-propargyl-puromycin and stable isotope-labelled amino acids. *J. Biochem.* **169**, 227–236 (2021).

18. Uchiyama, J. *et al.* pSNAP: Proteome-wide analysis of elongating nascent polypeptide chains. *iScience* **25**, 104516 (2022).

19. Kiick, K. L., Saxon, E., Tirrell, D. A. & Bertozzi, C. R. Incorporation of azides into recombinant proteins for chemoselective modification by the Staudinger ligation. *Proc. Natl. Acad. Sci. U. S. A.*

bioRxiv preprint doi: https://doi.org/10.1101/2023.03.03.530942; this version posted March 3, 2023. The copyright holder for this preprint (which was not certified by peer review) is the author/funder, who has granted bioRxiv a license to display the preprint in perpetuity. It is made available under aCC-BY-NC-ND 4.0 International license.

99, 19–24 (2002).

20. Van Hest, J. C. M., Kiick, K. L. & Tirrell, D. A. Efficient incorporation of unsaturated methionine analogues into proteins in vivo. *J. Am. Chem. Soc.* **122**, 1282–1288 (2000).

21. Ngo, J. T. *et al.* Cell-selective metabolic labeling of proteins. *Nat. Chem. Biol.* **5**, 715–717 (2009).

22. Dieterich, D. C., Link, A. J., Graumann, J., Tirrell, D. A. & Schuman, E. M. Selective identification of newly synthesized proteins in mammalian cells using bioorthogonal noncanonical amino acid tagging (BONCAT). *Proc. Natl. Acad. Sci.* (2006). doi:10.1073/pnas.0601637103

23. Howden, A. J. M. *et al.* QuaNCAT: Quantitating proteome dynamics in primary cells. *Nat. Methods* **10**, 343–346 (2013).

24. Kleinpenning, F., Steigenberger, B., Wu, W. & Heck, A. J. R. Fishing for newly synthesized proteins with phosphonate-handles. *Nat. Commun.* **11**, (2020).

25. Hong, V., Presolski, S. I., Ma, C. & Finn, M. G. Analysis and Optimization of Copper-Catalyzed Azide – Alkyne Cycloaddition for Bioconjugation **. *Angew. Chemie* 9879–9883 (2009). doi:10.1002/anie.200905087

26. Ma, Y., McClatchy, D. B., Barkallah, S., Wood, W. W. & Yates, J. R. Quantitative analysis of newly synthesized proteins. *Nat. Protoc.* **13**, 1744–1762 (2018).

27. Eichelbaum, K., Winter, M., Diaz, M. B., Herzig, S. & Krijgsveld, J. Selective enrichment of newly synthesized proteins for quantitative secretome analysis. *Nat. Biotechnol.* **30**, (2012).

28. Zhang, G. *et al.* In-depth quantitative proteomic analysis of de novo protein synthesis induced by brain-derived neurotrophic factor. *J. Proteome Res.* **13**, 5707–5714 (2014).

29. Bagert, J. D. *et al.* Quantitative, time-resolved proteomic analysis by combining bioorthogonal noncanonical amino acid tagging and pulsed stable isotope labeling by amino acids in cell culture. *Mol. Cell. Proteomics* **13**, 1352–1358 (2014).

30. Rothenberg, D. A. *et al.* A Proteomics Approach to Profiling the Temporal Translational Response to Stress and Growth. *iScience* **9**, 367–381 (2018).

31. Elder, M. K. *et al.* Age-dependent shift in the de novo proteome accompanies pathogenesis in an Alzheimer's disease mouse model. *Commun. Biol.* **4**, (2021).

32. Ma, Y., McClatchy, D. B., Martínez-Bartolomé, S., Bamberger, C. & Yates, J. R. Temporal Quantitative Profiling of Newly Synthesized Proteins during Aβ Accumulation. *J. Proteome Res.* **20**, 763–775 (2021).

33. Kuhn, T. C. *et al.* Secretome Analysis of Cardiomyocytes Identifies PCSK6 (Proprotein Convertase Subtilisin/Kexin Type 6) as a Novel Player in Cardiac Remodeling After Myocardial Infarction. *Circulation* **141**, 1628–1644 (2020).

34. Pauli, C. *et al.* Site-specific methylation of 18S ribosomal RNA by SNORD42A is required for acute myeloid leukemia cell proliferation. *Blood* **135**, 2059–2070 (2020).

35. Zhou, F. *et al.* A Dynamic rRNA Ribomethylome Drives Stemness in Acute Myeloid Leukemia. *Cancer Discov.* OF1–OF17 (2023). doi:10.1158/2159-8290.cd-22-0210

36. Hisaoka, M. *et al.* Preferential translation of p53 target genes. *RNA Biol.* **19**, 437–452 (2022).

37. Vargas-diaz, D. & Altelaar, M. Automated High-Throughput Method for the Fast, Robust, and Reproducible Enrichment of Newly Synthesized Proteins. *J. Proteome Res.* (2022). doi:10.1021/acs.jproteome.1c00743

38. Savitski, M. M. *et al.* Multiplexed Proteome Dynamics Profiling Reveals Mechanisms Controlling Protein Homeostasis. *Cell* **173**, 260-274.e25 (2018).

bioRxiv preprint doi: https://doi.org/10.1101/2023.03.03.530942; this version posted March 3, 2023. The copyright holder for this preprint (which was not certified by peer review) is the author/funder, who has granted bioRxiv a license to display the preprint in perpetuity. It is made available under aCC-BY-NC-ND 4.0 International license.

39. Klann, K., Tascher, G. & Münch, C. Functional Translatome Proteomics Reveal Converging and Dose-Dependent Regulation by mTORC1 and eIF2α. *Mol. Cell* **77**, 913-925.e4 (2020).

40. Kitata, R. B., Yang, J. C. & Chen, Y. J. Advances in data-independent acquisition mass spectrometry towards comprehensive digital proteome landscape. *Mass Spectrometry Reviews* (2022). doi:10.1002/mas.21781

41. Pino, L. K., Baeza, J., Lauman, R., Schilling, B. & Garcia, B. A. Improved SILAC quantification with data independent acquisition to investigate bortezomib-induced protein degradation. *J. Proteome Res.* (2020). doi:10.1101/2020.11.23.394304

42. Salovska, B., Li, W., Di, Y. & Liu, Y. BoxCarmax: A High-Selectivity Data-Independent Acquisition Mass Spectrometry Method for the Analysis of Protein Turnover and Complex Samples. *Anal. Chem.* (2021). doi:10.1021/acs.analchem.0c04293

43. Salovska, B. *et al.* Isoform-resolved correlation analysis between mRNA abundance regulation and protein level degradation . *Mol. Syst. Biol.* **16**, (2020).

44. Derks, J. *et al.* Increasing the throughput of sensitive proteomics by plexDIA. *Nat. Biotechnol.* (2022). doi:10.1038/s41587-022-01389-w

45. Müller, T. *et al.* Automated sample preparation with SP3 for low-input clinical proteomics. *Mol. Syst. Biol.* **16**, 1–19 (2020).

46. Demichev, V., Messner, C. B., Vernardis, S. I., Lilley, K. S. & Ralser, M. DIA-NN: neural networks and interference correction enable deep proteome coverage in high throughput. *Nat. Methods* **17**, 41–44 (2020).

47. Siwek, W., Tehrani, S. S. H., Mata, J. F. & Jansen, L. E. T. Activation of Clustered IFNγ Target Genes Drives Cohesin-Controlled Transcriptional Memory. *Mol. Cell* **80**, 396-409.e6 (2020).

48. Rusinova, I. *et al.* INTERFEROME v2.0: An updated database of annotated interferon-regulated genes. *Nucleic Acids Res.* **41**, 1040–1046 (2013).

49. Turner, J. & Crossley, M. Basic Krüppel-like factor functions within a network of interacting haematopoietic transcription factors. *Int. J. Biochem. Cell Biol.* **31**, 1169–1174 (1999).

50. Cantor, D. J. & David, G. The chromatin-associated Sin3B protein is required for hematopoietic stem cell functions in mice. *Blood* **129**, 60–70 (2017).

51. Ulgiati, D., Subrata, L. S. & Abraham, L. J. The role of Sp family members, basic Kruppel-like factor, and E box factors in the basal and IFN-gamma regulated expression of the human complement C4 promoter. *J. Immunol.* **164**, 300–307 (2000).

52. Weng, X. *et al.* Sin3B mediates collagen type I gene repression by interferon gamma in vascular smooth muscle cells. *Biochem. Biophys. Res. Commun.* **447**, 263–270 (2014).

53. Shirazi, Y. & Pitha, P. M. Interferon downregulates CXCR4 (fusin) gene expression in peripheral blood mononuclear cells. *J. Hum. Virol.* **1**, 69–76 (1998).

54. Dharan, A. *et al.* Bicaudal D2 facilitates the cytoplasmic trafficking and nuclear import of HIV-1 genomes during infection. *Proc. Natl. Acad. Sci. U. S. A.* **114**, E10707–E10716 (2017).

55. Lerchenmüller, C. *et al.* S100A6 regulates endothelial cell cycle progression by attenuating antiproliferative signal transducers and activators of transcription 1 signaling. *Arterioscler. Thromb. Vasc. Biol.* **36**, 1854–1867 (2016).

56. Begitt, A., Droescher, M., Knobeloch, K. P. & Vinkemeier, U. SUMO conjugation of STAT1 protects cells from hyperresponsiveness to IFNγ. *Blood* **118**, 1002–1007 (2011).

57. Shao, Y. *et al.* Enhancing Comprehensive Analysis of Newly Synthesized Proteins Based on

bioRxiv preprint doi: https://doi.org/10.1101/2023.03.03.530942; this version posted March 3, 2023. The copyright holder for this preprint (which was not certified by peer review) is the author/funder, who has granted bioRxiv a license to display the preprint in perpetuity. It is made available under aCC-BY-NC-ND 4.0 International license.

Cleavable Bioorthogonal Tagging. *Anal. Chem.* (2021). doi:10.1021/acs.analchem.1c00965

58. Yang, Y., Grammel, M., Raghavan, A. S., Charron, G. & Hang, H. C. Article Comparative Analysis of Cleavable Azobenzene-Based Affinity Tags for Bioorthogonal Chemical Proteomics. *Chem. Biol.* **17**, 1212–1222 (2010).

59. Skowronek, P., Wahle, M., Zeng, W. & Zhou, X. Robust dimethyl-based multiplex-DIA workflow doubles single-cell proteome depth via a reference channel Author list. *bioRxiv* 1–51 (2022).

60. Vargas-Diaz, D. & Altelaar, M. Automated High-Throughput Method for the Fast, Robust, and Reproducible Enrichment of Newly Synthesized Proteins. *J. Proteome Res.* **21**, 189–199 (2022).

61. Ekkebus, R. *et al.* On terminal alkynes that can react with active-site cysteine nucleophiles in proteases. *J. Am. Chem. Soc.* **135**, 2867–2870 (2013).

62. Rostovtsev, V. V, Green, L. G., Fokin, V. V & Sharpless, K. B. A stepwise huisgen cycloaddition process: Copper(I)-catalyzed regioselective 'ligation' of azides and terminal alkynes. *Angew. Chemie - Int. Ed.* **41**, 2596–2599 (2002).

63. Tornøe, C. W., Christensen, C. & Meldal, M. Peptidotriazoles on solid phase: [1,2,3]-Triazoles by regiospecific copper(I)-catalyzed 1,3-dipolar cycloadditions of terminal alkynes to azides. *J. Org. Chem.* **67**, 3057–3064 (2002).

64. Hughes, C. S. *et al.* Ultrasensitive proteome analysis using paramagnetic bead technology. *Mol. Syst. Biol.* **10**, 757 (2014).

65. Cox, J. & Mann, M. MaxQuant enables high peptide identification rates, individualized p.p.b.-range mass accuracies and proteome-wide protein quantification. *Nat. Biotechnol.* **26**, 1367–1372 (2008).

66. Frankenfield, A. M., Ni, J., Ahmed, M. & Hao, L. Protein Contaminants Matter: Building Universal Protein Contaminant Libraries for DDA and DIA Proteomics. *J. Proteome Res.* (2022). doi:10.1021/acs.jproteome.2c00145

67. Pham, T. V., Henneman, A. A. & Jimenez, C. R. Iq: An R package to estimate relative protein abundances from ion quantification in DIA-MS-based proteomics. *Bioinformatics* **36**, 2611–2613 (2020).

68. Ritchie, M. E. *et al.* limma powers differential expression analyses for RNA-sequencing and microarray studies. *Nucleic Acids Res.* **43**, (2015).

69. Zhu, Y. *et al.* DEqMS: a method for accurate variance estimation in differential protein expression analysis. *Mol. Cell. Proteomics* mcp.TIR119.001646 (2020). doi:10.1074/mcp.tir119.001646

70. Wu, T. *et al.* clusterProfiler 4.0: A universal enrichment tool for interpreting omics data. *Innovation(China)* **2**, 100141 (2021).

71. Liberzon, A. *et al.* The Molecular Signatures Database Hallmark Gene Set Collection. *Cell Syst.* **1**, 417–425 (2015).

72. Luo, Y. *et al.* New developments on the Encyclopedia of DNA Elements (ENCODE) data portal. *Nucleic Acids Res.* **48**, D882–D889 (2020).

73. Benjamini, Y. & Hochberg, Y. Controlling the False Discovery Rate: A Practical and Powerful Approach to Multiple Testing. *J. R. Stat. Soc. Ser. B* **57**, 289–300 (1995).

74. Perez-Riverol, Y. *et al.* The PRIDE database resources in 2022: A hub for mass spectrometry-based proteomics evidences. *Nucleic Acids Res.* **50**, D543–D552 (2022).

bioRxiv preprint doi: https://doi.org/10.1101/2023.03.03.530942; this version posted March 3, 2023. The copyright holder for this preprint (which was not certified by peer review) is the author/funder, who has granted bioRxiv a license to display the preprint in perpetuity. It is made available under aCC-BY-NC-ND 4.0 International license.

Figure legends

Figure 1

Schematic representation of the workflow for quantitative newly synthesized proteome analysis with automated sample preparation (QuaNPA). The workflow consists of four main steps. 1. In preparation for the enrichment of newly synthesized proteins (NSP), epoxy-activated magnetic alkyne agarose beads are coupled with propargylamine to produce magnetic alkyne agarose (MAA) beads. 2. Metabolic labelling of NSPs in cultured cells is carried out with L-azidohomoalanine (AHA) and heavy- and intermediate stable isotope-labelled Lysine and Arginine. Cells with different treatment conditions are mixed and lysed by AFA sonication. 3. NSPs are enriched by covalent coupling to MAA beads via click-chemistry on a Bravo robotic liquid handling platform. NSPs are digested off the MAA beads and purified using the autoSP3 protocol. 4. NSPs are characterized by mass spectrometry via data-dependent or data-independent acquisition (DDA or DIA, respectively), and data analysis is carried out with DDA search engines such as Maxquant or DIA-NN and plexDIA for DIA data. This graphic was created in part with Biorender.

Figure 2

Preparation and use of magnetic alkyne agarose (MAA) beads. A) Epoxy-activated magnetic agarose beads are coupled with propargylamine to produce MAA beads. B) AHA-containing proteins are covalently bound to MAA beads using click chemistry (Cu(I)-catalyzed azide alkyne cycloaddition (CuAAC)).

Figure 3

Optimizing the semi-automated enrichment of newly synthesized proteins via QuaNPA. Performance was evaluated when using different MAA bead volumes (panel A-D) and amounts of protein input (panel E-F). A) Intensity ratios of heavy- and intermediate SILAC labelled precursors (originating from newly synthesized proteins), over light precursor ions (originating from pre-existing proteins). The upper and lower whiskers, of the ratio boxplots, extend from the hinges to the highest or lowest values that are within 1.5x the interquartile range. B) Number of quantified protein groups (with heavy- over intermediate SILAC ratio). Numbers indicate the average of 2 replicates (grey dots). C) Boxplot indicating the log2 SILAC H/M ratios of the individual protein groups. The upper and lower whiskers extend from the hinges to the highest or lowest values that are within 1.5x the interquartile range. Values outside this range are plotted as dots and represent outliers. The expected log2 SILAC ratio is 0. D) Coefficient of variation (CV) values of the SILAC H/M ratios of the quantified protein groups. E) Intensity ratios of heavy- and intermediate SILAC labelled precursors, from NSP samples prepared with different amounts of protein input. The upper and lower whiskers, of the ratio boxplots, extend from the hinges to the highest or lowest values that are within 1.5x the interquartile range. F) Number of quantified protein groups across the input dilution series. Data based on 2 experimental replicates. nE: non-enriched NSP sample.

bioRxiv preprint doi: https://doi.org/10.1101/2023.03.03.530942; this version posted March 3, 2023. The copyright holder for this preprint (which was not certified by peer review) is the author/funder, who has granted bioRxiv a license to display the preprint in perpetuity. It is made available under aCC-BY-NC-ND 4.0 International license.

Figure 4

Comparative analysis of SILAC labelled benchmark samples using data-dependent acquisition (DDA) and data-independent acquisition (DIA) mass spectrometry. A) Schematic representation of the composition of the SILAC labelled Hela samples. B) Schematic representation of the top 20 DDA method and the two DIA methods, which were used for the analysis. The maximum cycle time for each method is indicated in brackets. C) Comparison of the number of quantified protein groups for the different methods, with values based on MS1-based quantification in blue and MS2-based quantification indicated in red. Numbers indicate the average of 3 replicates (indicated individually with dots and triangles). D) Boxplot indicating coefficient of variation (CV) values of the SILAC ratios of the quantified protein groups, with values based on MS1-based quantification in blue and MS2-based quantification indicated in red. Median values are indicated below the boxplots. The upper and lower whiskers extend from the hinges to the highest or lowest values that are within 1.5x the interquartile range. Values outside this range are plotted as dots and represent outliers. E) Boxplots indicating the distribution of log2-transformed SILAC ratios of the quantified protein groups, with values based on MS1-based quantification in blue and MS2-based quantification indicated in red. The median of the difference from the theoretical log2 ratio is indicated below the boxplots. Upper and lower whiskers extend from the hinges to the highest or lowest values that are within 1.5x the interquartile range. Values outside this range are plotted as dots and represent outliers. Data based on 3 technical replicates of the single SILAC mix samples.

Figure 5

Analysis of newly synthesized proteins in Hela cells in response to treatment with interferon gamma (IFNg). A) Schematic representation of the experimental design and analysis workflow. B) Number of quantified protein groups in the samples with the indicated IFNg treatment time points. Numbers indicate the average of three replicates (indicated individually with black dots). C) Boxplots indicating the coefficient of Variation (CV) values of the quantified protein groups for each time point. Upper and lower whiskers extend from the hinges to the highest or lowest values that are within 1.5x the interquartile range. Values outside this range are plotted as dots and represent outliers. D) Principal component analysis (PCA) of the NSP samples. E) Volcano plots of the IFNg-induced changes in the newly synthesized proteome. Significantly upregulated proteins (adjusted p-value < 0.05 and log2 fold change > 0.585) are highlighted in red and significantly downregulated protein (adjusted p-value < 0.05 and log2 fold change < -0.585) are highlighted in blue. Only unique protein groups were included in the differential expression analysis. F) Dot plot highlighting overrepresented sets of proteins, which are significantly upregulated in response to IFNg at the indicated time points (q-value < 0.05). Data based on 3 experimental replicates.

Figure 6

Heatmap of newly synthesized proteins with differential expression in response to IFNg treatment. The subset of differentially expressed proteins (absolute log2 fold change > 1 and adj. p-value < 0.05, at any of the 5 time points and CV < 20 % across all time points) was selected and classified into three groups depending on the earliest time point in the time course their change in expression reached statistical significance (abs. log2 fold change > 0.585 and adj. p-value < 0.05) (early: 2h; intermediate: 4-9h; late: 24h). Significant changes in newly synthesized protein abundance are indicates with black outline in the cells of the heatmap and the colour gradient indicates the log2 fold change values of the proteins. The bar graph indicated the number of datasets in the interferome database, in which a fold change >2 or <0.5 was reported in human cells or tissues for the respective protein or gene. The asterisk sign (*) on top of bars indicates whether the protein is listed in the response to IFNg Hallmark or GO-term.

bioRxiv preprint doi: https://doi.org/10.1101/2023.03.03.530942; this version posted March 3, 2023. The copyright holder for this preprint (which was not certified by peer review) is the author/funder, who has granted bioRxiv a license to display the preprint in perpetuity. It is made available under aCC-BY-NC-ND 4.0 International license.

Supplementary figure 1

Schematic overview of the Bravo liquid handling platform deck for the automated NSP enrichment and SP3 peptide purification (A) and recovery step of tryptic peptides (B).

Supplementary figure 2

Protein metrics of pulse-labeled samples analysed by mass spectrometry with and without prior enrichment of NSPs. A) Ratios of labelled NSPs over unlabelled pre-existing proteins, of enriched newly synthesized proteome samples and samples prepared without NSP enrichment plotted against the summed intensity. B) Scatter plot of the precursor ratios of NSPs over pre-existing proteins, and the respective peptide hydrophobicity (GRAVY index), in enriched newly synthesized proteome samples and samples prepared without NSP enrichment. Data show that NSPs span the full range in the GRAVY index. C) Boxplots of SILAC ratios of newly synthesized proteome samples generated with different amounts of protein input. H- and M-labelled samples were mixed in equal amounts, to produce an expected log2 H/M ratio of 0. Upper and lower whiskers of the boxplots extend from the hinges to the highest or lowest values that are within 1.5x the interquartile range. Values outside this range are plotted as dots and represent outliers. D) Boxplots indicating the coefficient of variation (CV) values calculated from the SILAC ratios of NSP samples that were prepared with different amounts of protein input. Upper and lower whiskers extend from the hinges to the highest or lowest values that are within 1.5x the interquartile range. Values outside this range are plotted as dots and represent outliers. Data based on 2 experimental replicates.

Supplementary figure 3

Representative chromatograms of NSP samples, with (left panels) and without (right panels) enrichment of NSPs via click-chemistry. LCMS analyses used identical LC gradients and mass spectrometer settings. A) Base peak- and B) Total ion current (TIC) chromatogram.

Supplementary figure 4

Comparison of NSP data of IFNg-treated Hela cells, obtained with the QuaNPA workflow and with PhosID [24]. A) MA plots of newly synthesized proteome data of IFNg treated Hela cells, generated with the PhosID and QuaNPA workflow at two time points. The number of quantified proteins and differentially expressed proteins (adj. p-value < 0.05 & absolute log2FC > 0.585) are highlighted. Only unique protein groups from the samples generated with the QuaNPA workflow were included. PhosID samples were generated with 500 µg protein input and were measured using a 120 min method on an Orbitrap Fusion mass spectrometer (ThermoFischer). QuaNPA samples were generated from 100 µg protein input and measured using a 90 min method on a QExactive HF mass spectrometer (ThermoFischer). B) Dotplot representing GSEA results of the NSP data generated with the 2 methods. Only significantly enriched protein sets (q-value < 0.05) are included in the graph. Data based on 3 experimental replicates.

Supplementary figure 5

Log2-transformed fold change values of the newly synthesized proteome (NSP) data and published RNAseq data of Hela cells treated with IFNg for 24 h [47], displayed in scatter plots. A) Correlation (Pearson) of the complete transcriptome and NSP data. B) Correlation (Pearson) of the subset of differentially expressed NSP subset (adj. p-value < 0.05 & abs(log2FC > 0.585)) and the respective transcriptomic data. C) Correlation (Pearson) of the subset of differentially expressed mRNA subset (adj. p-value < 0.05 &

bioRxiv preprint doi: https://doi.org/10.1101/2023.03.03.530942; this version posted March 3, 2023. The copyright holder for this preprint (which was not certified by peer review) is the author/funder, who has granted bioRxiv a license to display the preprint in perpetuity. It is made available under aCC-BY-NC-ND 4.0 International license.

968 abs(log2FC > 0.585)) and the respective NSP data. D) Correlation (Pearson) of the subset of NSP and
969 mRNA that are STAT1 ChIPseq targets in Hela cells treated with IFNg for 30 min.

970

bioRxiv preprint doi: https://doi.org/10.1101/2023.03.03.530942; this version posted March 3, 2023. The copyright holder for this preprint (which was not certified by peer review) is the author/funder, who has granted bioRxiv a license to display the preprint in perpetuity. It is made available under aCC-BY-NC-ND 4.0 International license.

971 **Figures**

972

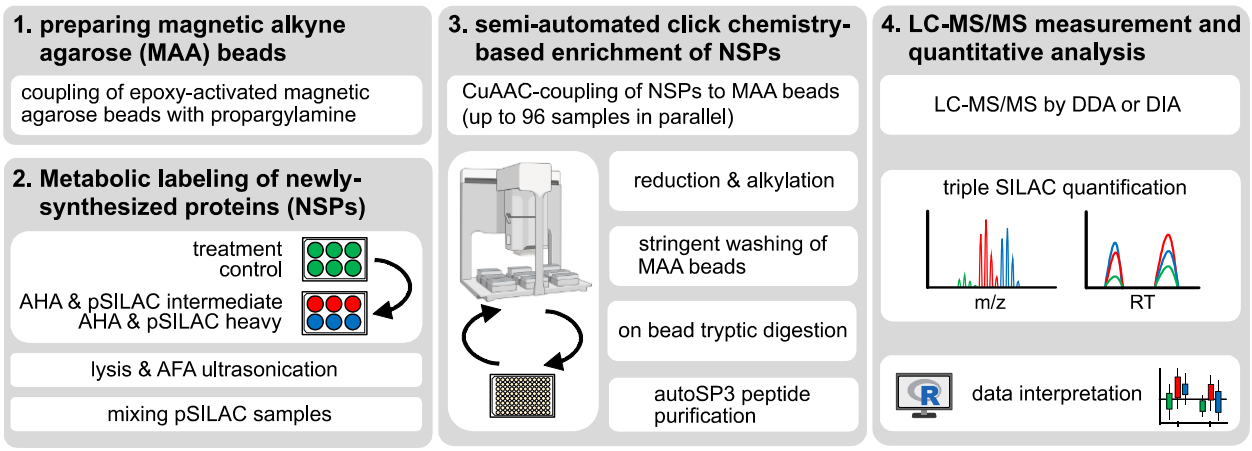

973

974 Figure 1

975

bioRxiv preprint doi: https://doi.org/10.1101/2023.03.03.530942; this version posted March 3, 2023. The copyright holder for this preprint (which was not certified by peer review) is the author/funder, who has granted bioRxiv a license to display the preprint in perpetuity. It is made available under aCC-BY-NC-ND 4.0 International license.

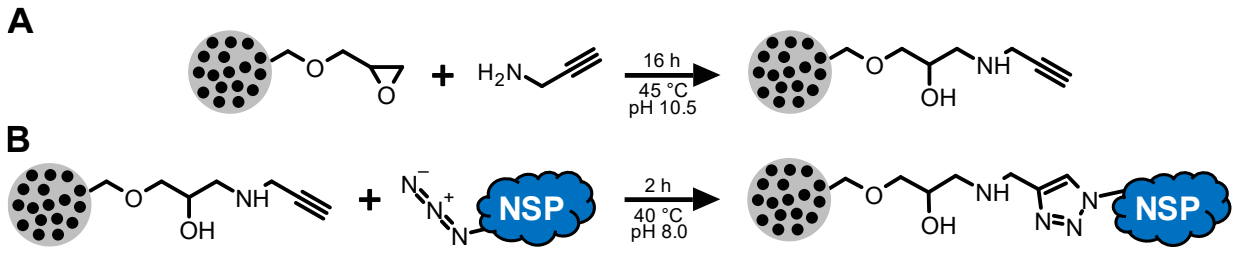

Figure 2

bioRxiv preprint doi: https://doi.org/10.1101/2023.03.03.530942; this version posted March 3, 2023. The copyright holder for this preprint (which was not certified by peer review) is the author/funder, who has granted bioRxiv a license to display the preprint in perpetuity. It is made available under aCC-BY-NC-ND 4.0 International license.

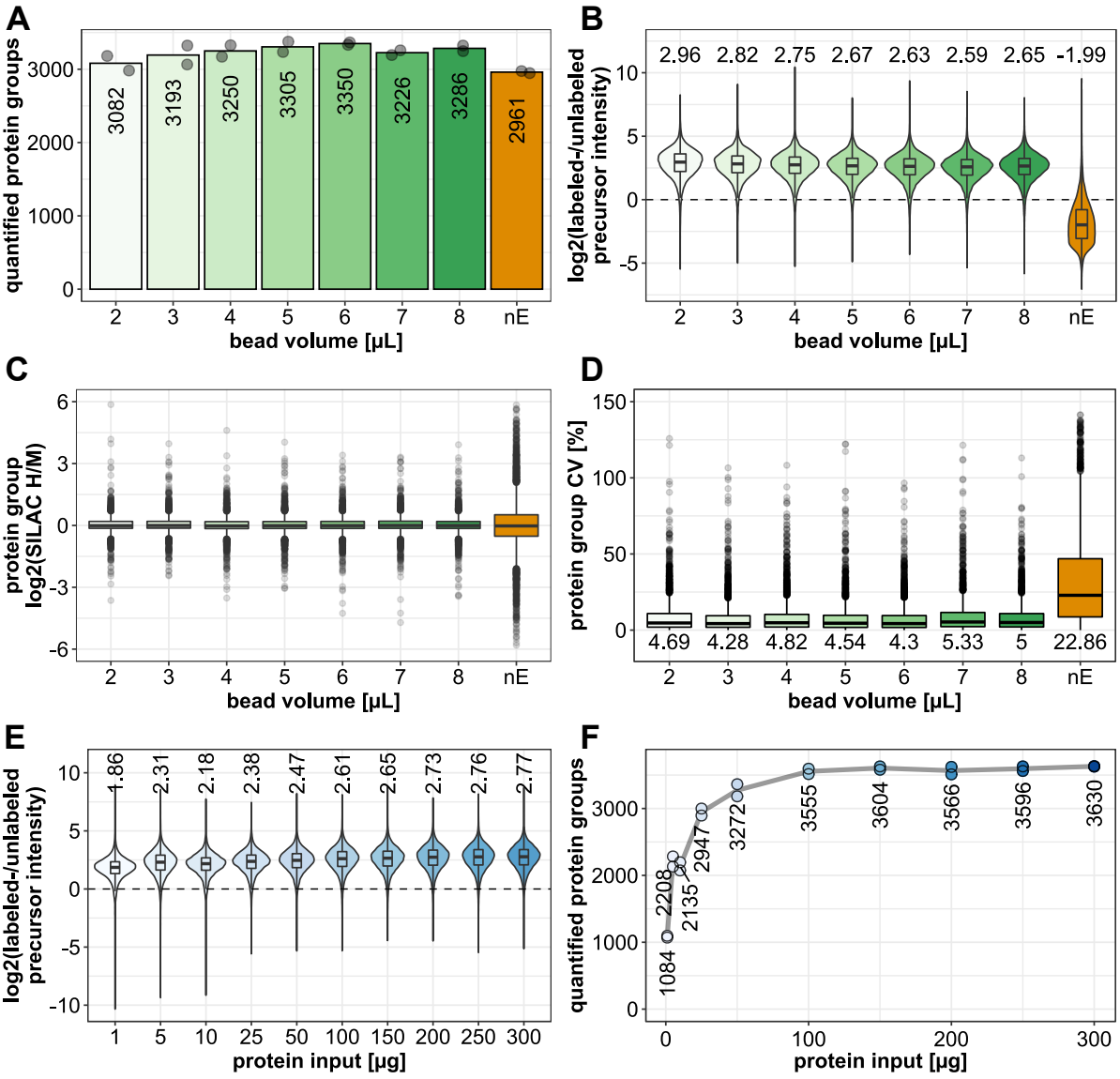

979

980 Figure 3

bioRxiv preprint doi: https://doi.org/10.1101/2023.03.03.530942; this version posted March 3, 2023. The copyright holder for this preprint (which was not certified by peer review) is the author/funder, who has granted bioRxiv a license to display the preprint in perpetuity. It is made available under aCC-BY-NC-ND 4.0 International license.

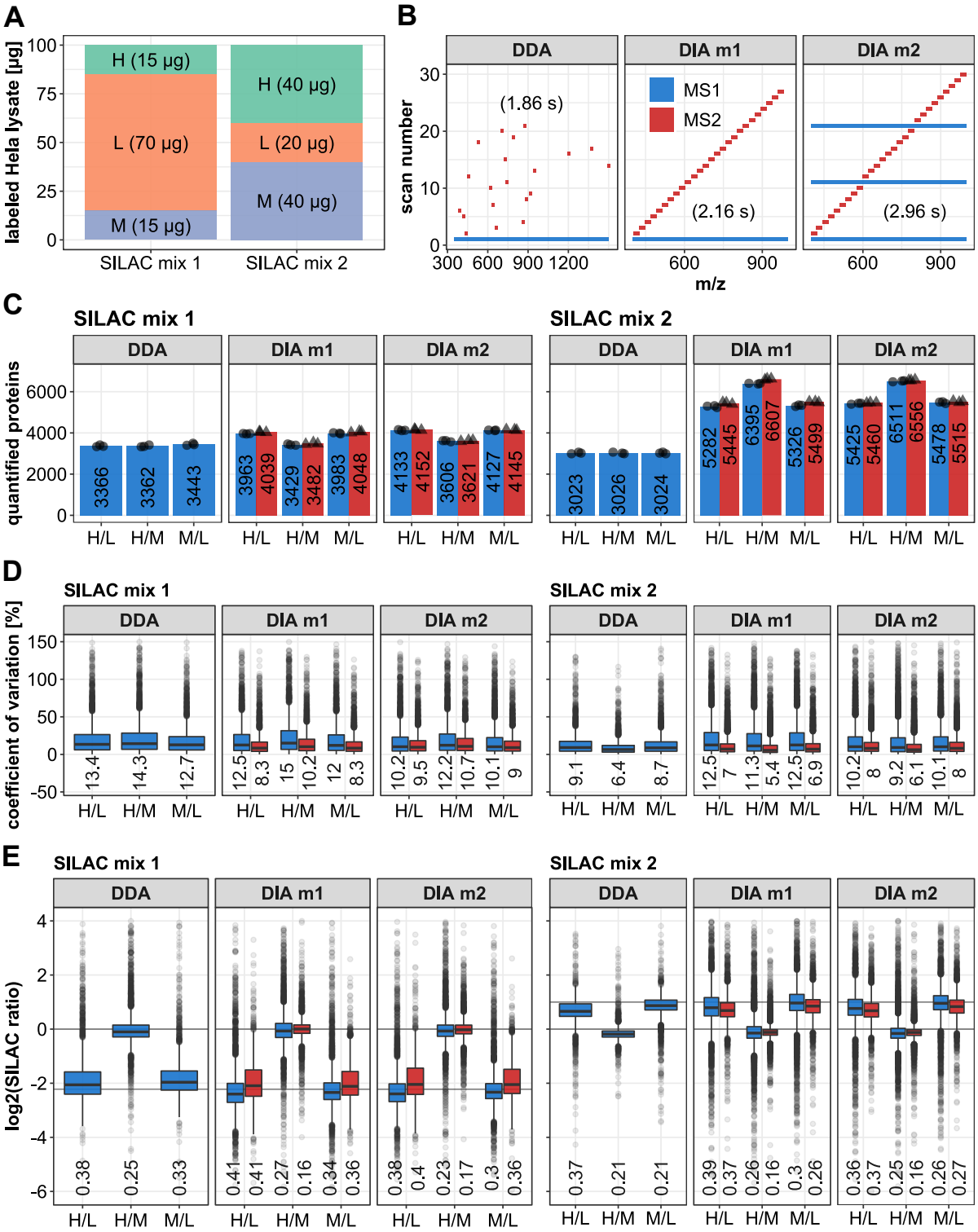

981

982 Figure 4

bioRxiv preprint doi: https://doi.org/10.1101/2023.03.03.530942; this version posted March 3, 2023. The copyright holder for this preprint (which was not certified by peer review) is the author/funder, who has granted bioRxiv a license to display the preprint in perpetuity. It is made available under aCC-BY-NC-ND 4.0 International license.

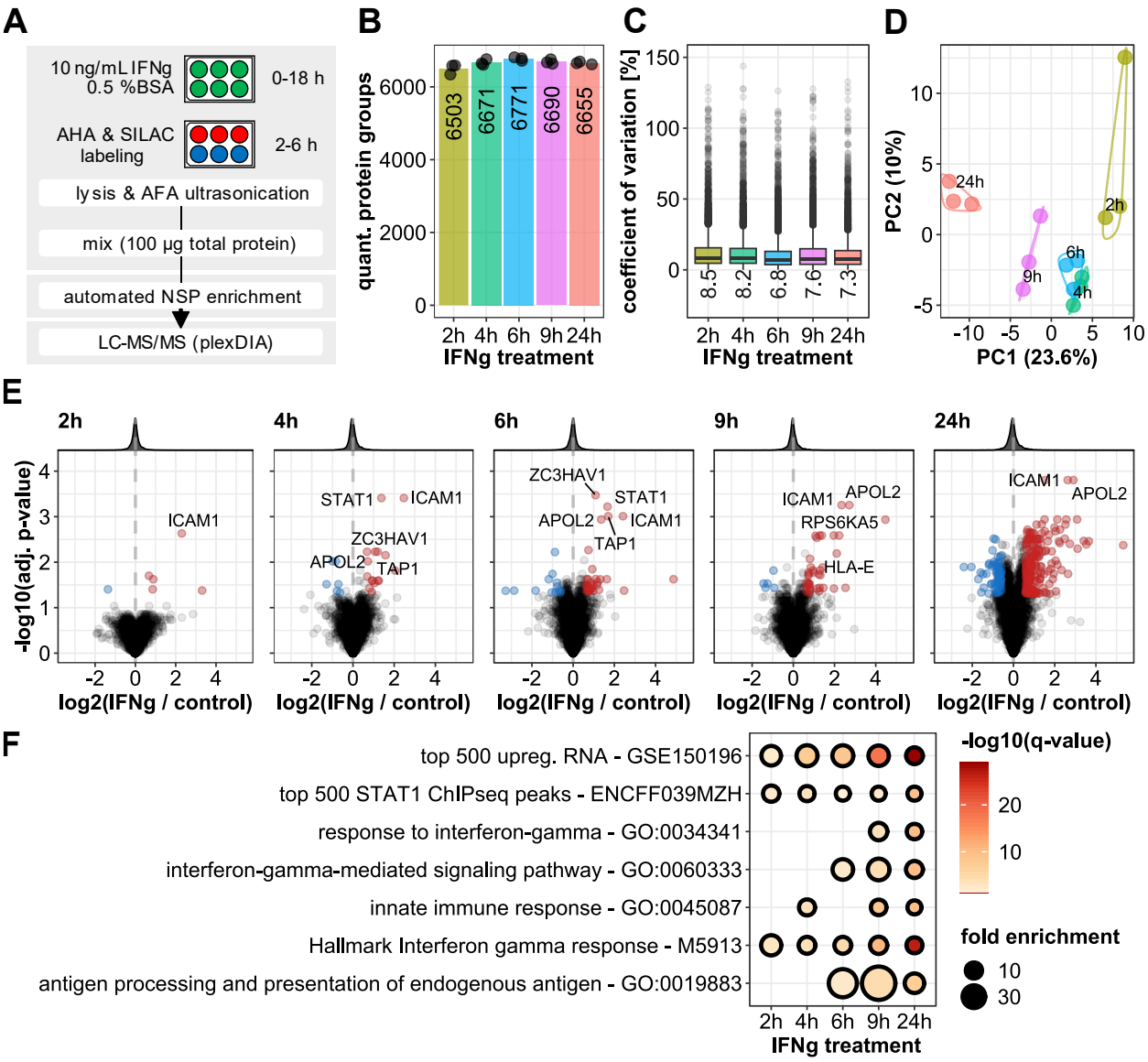

Figure 5

bioRxiv preprint doi: https://doi.org/10.1101/2023.03.03.530942; this version posted March 3, 2023. The copyright holder for this preprint (which was not certified by peer review) is the author/funder, who has granted bioRxiv a license to display the preprint in perpetuity. It is made available under aCC-BY-NC-ND 4.0 International license.

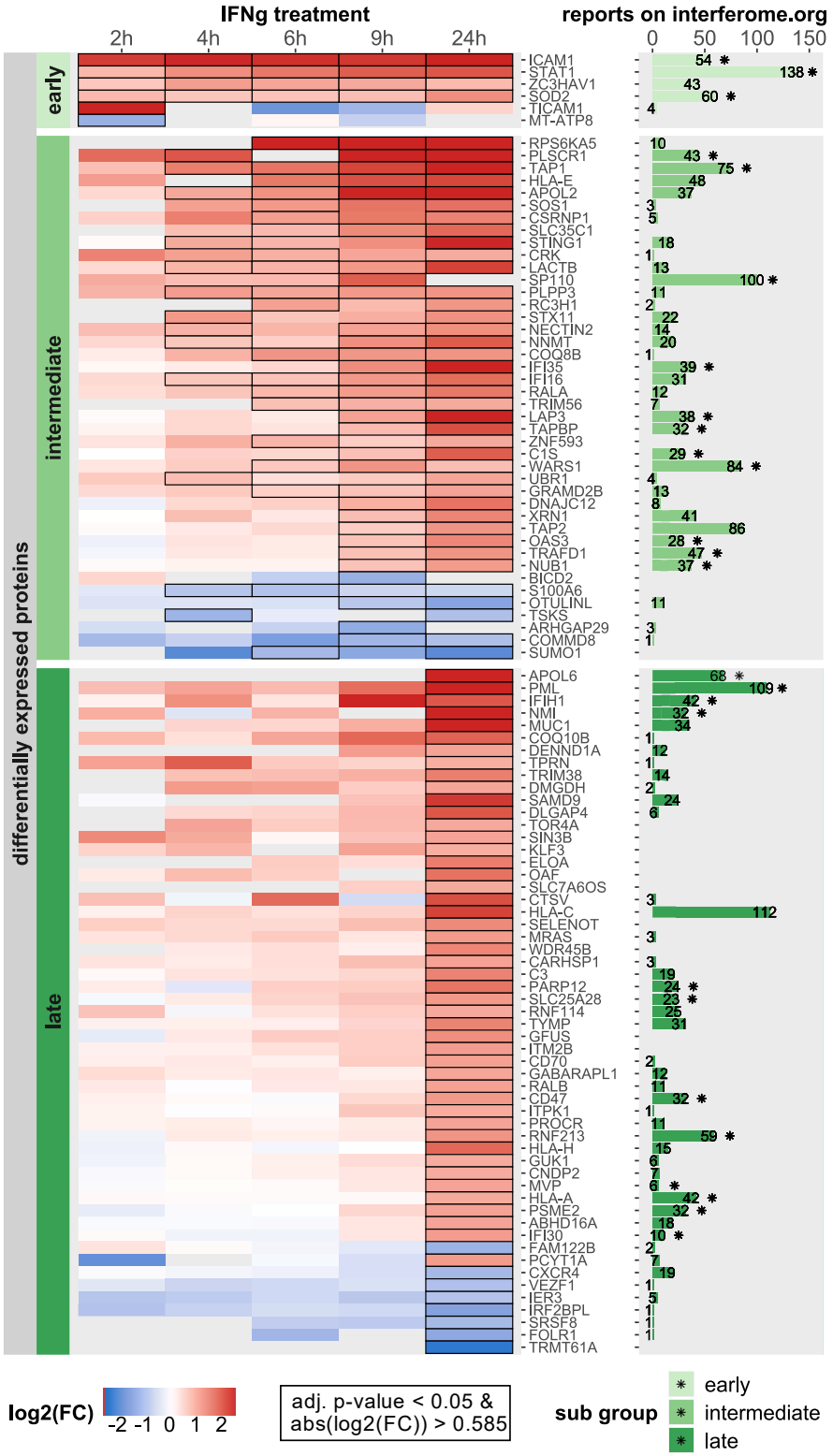

Figure 6

bioRxiv preprint doi: https://doi.org/10.1101/2023.03.03.530942; this version posted March 3, 2023. The copyright holder for this preprint (which was not certified by peer review) is the author/funder, who has granted bioRxiv a license to display the preprint in perpetuity. It is made available under aCC-BY-NC-ND 4.0 International license.

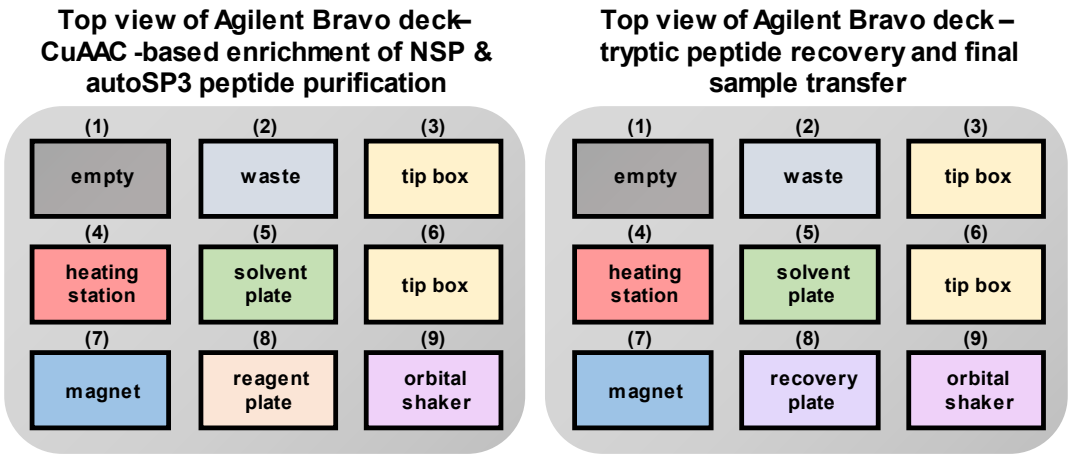

Supplementary figure 1

bioRxiv preprint doi: https://doi.org/10.1101/2023.03.03.530942; this version posted March 3, 2023. The copyright holder for this preprint (which was not certified by peer review) is the author/funder, who has granted bioRxiv a license to display the preprint in perpetuity. It is made available under aCC-BY-NC-ND 4.0 International license.

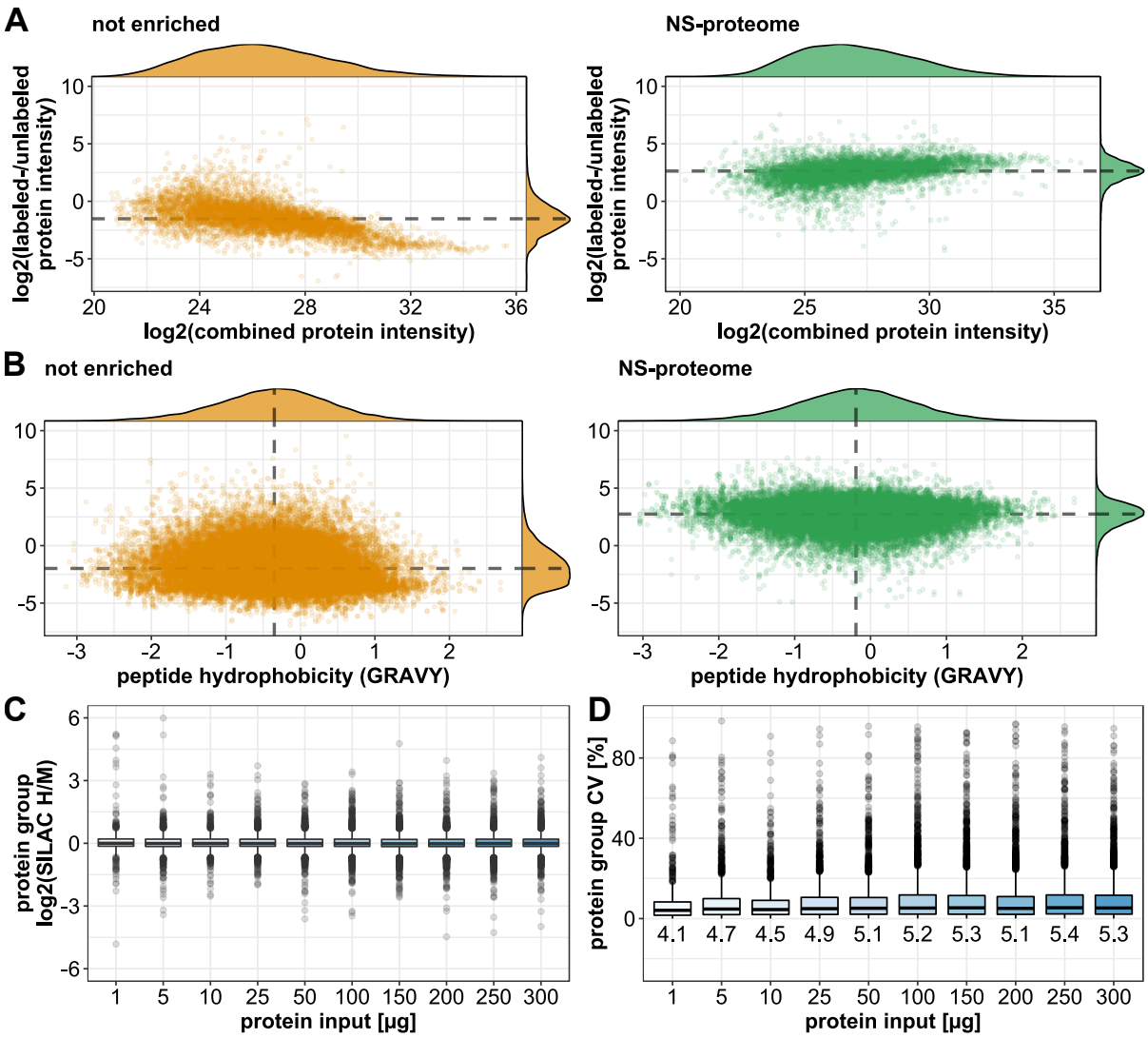

Supplementary figure 2

bioRxiv preprint doi: https://doi.org/10.1101/2023.03.03.530942; this version posted March 3, 2023. The copyright holder for this preprint (which was not certified by peer review) is the author/funder, who has granted bioRxiv a license to display the preprint in perpetuity. It is made available under aCC-BY-NC-ND 4.0 International license.

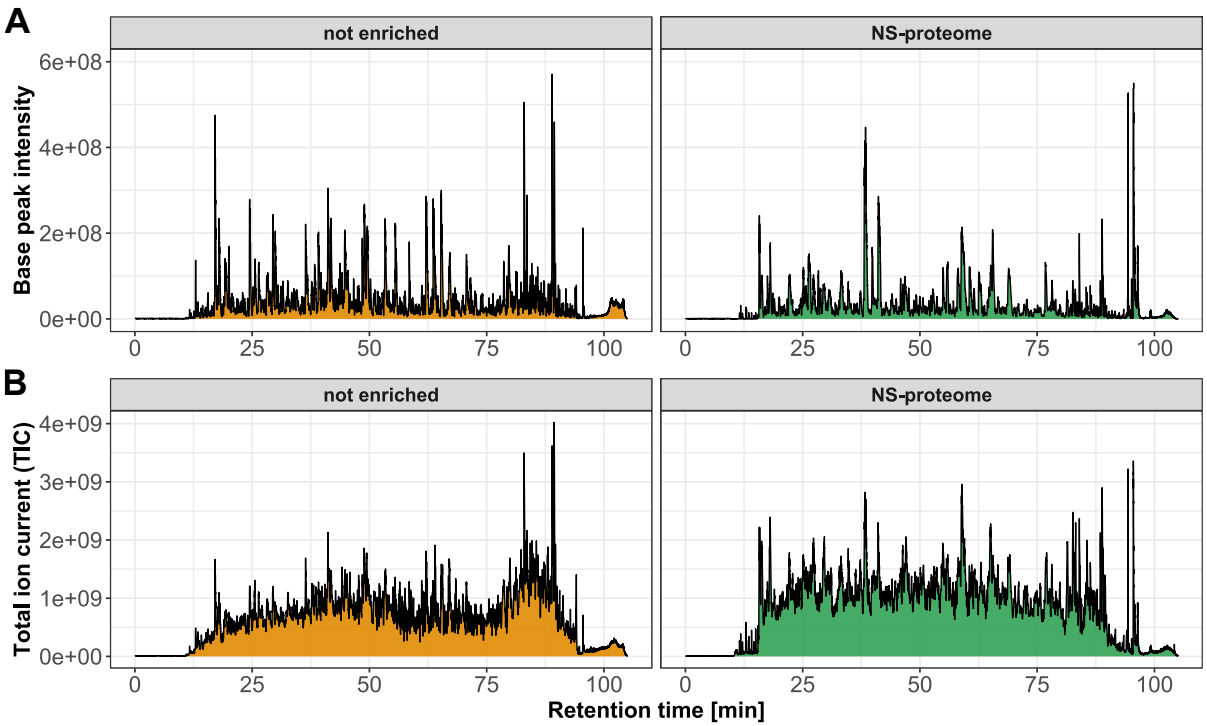

Supplementary figure 3

bioRxiv preprint doi: https://doi.org/10.1101/2023.03.03.530942; this version posted March 3, 2023. The copyright holder for this preprint (which was not certified by peer review) is the author/funder, who has granted bioRxiv a license to display the preprint in perpetuity. It is made available under aCC-BY-NC-ND 4.0 International license.

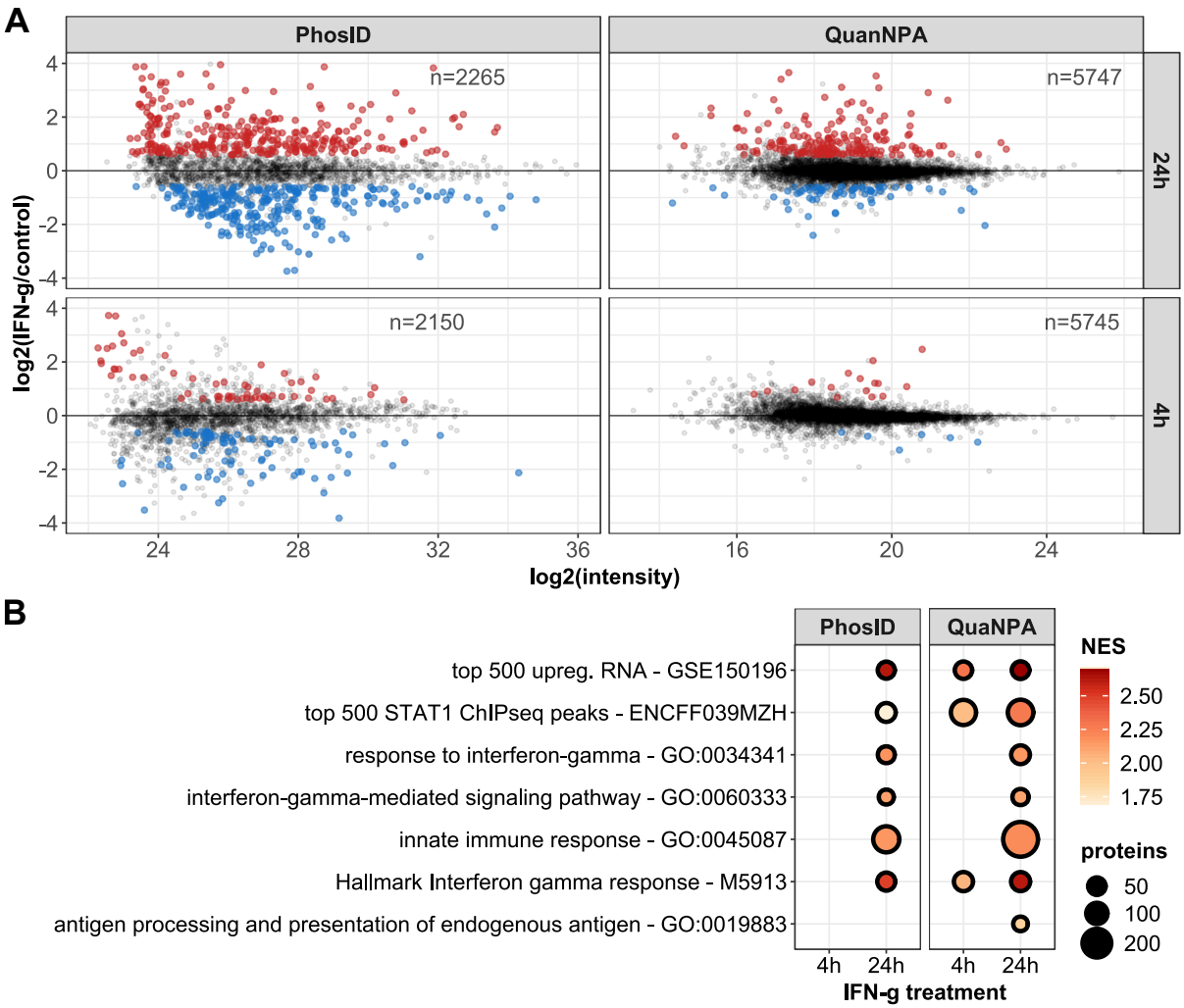

Supplementary figure 4

bioRxiv preprint doi: https://doi.org/10.1101/2023.03.03.530942; this version posted March 3, 2023. The copyright holder for this preprint (which was not certified by peer review) is the author/funder, who has granted bioRxiv a license to display the preprint in perpetuity. It is made available under aCC-BY-NC-ND 4.0 International license.

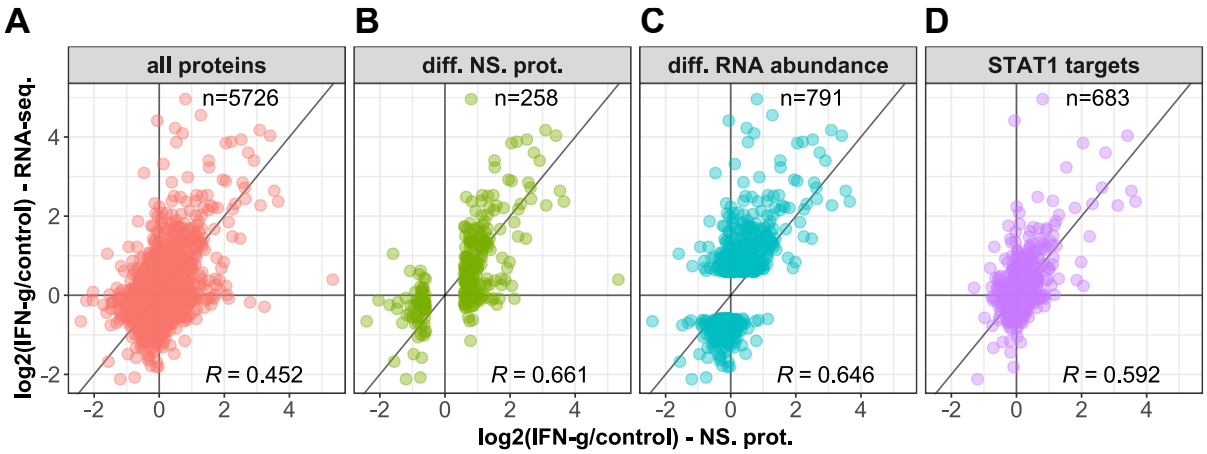

1001

1002 Supplementary figure 5